micromachines

Review

Titanium Carbide ($Ti_3C_2T_x$) MXene as Efficient Electron/Hole Transport Material for Perovskite Solar Cells and Electrode Material for Electrochemical Biosensors/Non-Biosensors Applications

Theophile Niyitanga [1], Archana Chaudhary [2,*], Khursheed Ahmad [1] and Haekyoung Kim [1,*]

[1] School of Materials Science and Engineering, Yeungnam University, Gyeongsan 38541, Republic of Korea
[2] Department of Chemistry, Medi-Caps University, Indore 453331, Madhya Pradesh, India
* Correspondence: archana.choudhary@medicaps.ac.in (A.C.); hkkimyu@yu.ac.kr (H.K.)

Abstract: Recently, two-dimensional (2D) MXenes materials have received enormous attention because of their excellent physiochemical properties such as high carrier mobility, metallic electrical conductivity, mechanical properties, transparency, and tunable work function. MXenes play a significant role as additives, charge transfer layers, and conductive electrodes for optoelectronic applications. Particularly, titanium carbide ($Ti_3C_2T_x$) MXene demonstrates excellent optoelectronic features, tunable work function, good electron affinity, and high conductivity. The $Ti_3C_2T_x$ has been widely used as electron transport (ETL) or hole transport layers (HTL) in the development of perovskite solar cells (PSCs). Additionally, $Ti_3C_2T_x$ has excellent electrochemical properties and has been widely explored as sensing material for the development of electrochemical biosensors. In this review article, we have summarized the recent advances in the development of the PSCs using $Ti_3C_2T_x$ MXene as ETL and HTL. We have also compiled the recent progress in the fabrication of biosensors using $Ti_3C_2T_x$-based electrode materials. We believed that the present mini review article would be useful to provide a deep understanding, and comprehensive insight into the research status.

Keywords: MXene; $Ti_3C_2T_x$; perovskite solar cells; electron transport layers; hole transport layers; electrochemical biosensors

Citation: Niyitanga, T.; Chaudhary, A.; Ahmad, K.; Kim, H. Titanium Carbide ($Ti_3C_2T_x$) MXene as Efficient Electron/Hole Transport Material for Perovskite Solar Cells and Electrode Material for Electrochemical Biosensors/Non-Biosensors Applications. *Micromachines* **2023**, *14*, 1907. https://doi.org/10.3390/mi14101907

Academic Editor: Antonella Battisti

Received: 31 August 2023
Revised: 30 September 2023
Accepted: 4 October 2023
Published: 6 October 2023

1. Introduction

In the present scenario, the design and fabrication of bi-functional or multi-functional materials received extensive attention for various optoelectronic and electrochemical applications [1–3]. It is of great significance to summarize the bi-functional properties of such materials towards the development of perovskite solar cells (PSCs) and electrochemical biosensors [4–6]. The PSCs have been proven as the most efficient thin film-based photovoltaic technology compared to the conventional solar cells [7–10]. The poor stability and low charge transport properties of the PSCs are the major concerns for the development of highly stable and high-performance PSCs [11]. Therefore, it has been considered that the stability and charge transport properties of the PSCs can be further enhanced by employing efficient electron/hole transport layers (ETL or HTL) [12,13]. Ding et al. [14] demonstrated the fabrication of tandem solar cells which exhibited a PCE of 21.4%. Chen et al. [15] also reported the enhanced photovoltaic performance of PSCs. Ma et al. [16] optimized the surface morphology and reported the improved photovoltaic performance. Chen et al. [17] reported the passivation and buried interface study of 2D perovskite on ETL and achieved good performance.

The two-dimensional (2D) layered materials such as carbon nitride, hexagonal boron nitride, black phosphorus, transition metal dichalcogenides, and hybrid materials have received enormous attention because of their excellent optoelectronic properties [18–20]. The

layered materials have been widely explored in various optoelectronic applications such as solar cells, supercapacitors, batteries, light emitting diodes, and photo-detectors [21–33]. Graphene has been proven as a highly efficient electrode material for various optoelectronic applications [34–45]. The 2D layered materials are promising material for their implantation in optoelectronic devices [17]. According to the reported literature, it was observed that the utilization of 2D materials enhanced the charge transport properties and reduced the recombination reactions [43]. The 2D layered materials can offer a perfect uniform surface due to the presence of the inherent confinement in the out-of-plane direction. Thus, 2D layered materials can be suitable as ETL or HTL for the fabrication of high-performance PSCs. Previously, various layered materials such as graphene, MoS_2, WS_2, SnS_2, and TiS_2, etc., have been reported in the development of PSCs. Tang et al. [45] reported the benign synthetic procedure for the preparation of MoS_2 and introduced it as ETL for the construction of PSCs. The introduction of MoS_2 significantly enhanced the photovoltaic performance of the fabricated PSCs and an interesting power conversion efficiency (PCE) of 20.55% was achieved. Other work also demonstrated the use of tungsten disulfide (WS_2) as ETL and reported a decent PCE of 12.44% [46].

Recently, Yin et al. [47] have proposed an exfoliation method for the preparation of titanium disulfide (TiS_2) films as ETL for the development of PSCs which demonstrated a PCE of 17.37%. Tin disulfide (SnS_2) has a CdI_2-like layered structure (where Sn atoms are sandwiched between two S atoms) and has been explored as ETL by Zhao et al. [48]. The aforementioned points show that layered materials can be used as efficient ETL or HTL materials to improve the PCE of the PSCs.

In 2011, Gogotsi and coworkers have discovered a new class of 2D materials which is known as MXenes [49]. In general, MXenes are a large family of 2D transition metal nitrides, carbonitrides, and carbides with the general chemical formula of $M_{n+1}X_nT_x$ (where n = 1, 2 or 3; M = transition metal such as Mo, Ti, Cr, Hf, Zr, Nb, Ta; X = C or N and T_x = surface functional group such as –OH, –O, –F, and –Cl) [50]. MXenes possess excellent physiochemical features such as tunable optical, mechanical, biological, and electrical properties, which makes them a suitable candidate for optoelectronic devices [51–53]. Among different MXenes, $Ti_3C_2T_x$ has attracted material scientists and electrochemists because of its high transparency, excellent electron mobility, thermal stability, and high electrical conductivity [54]. The work function of the $Ti_3C_2T_x$ MXene can be tuned from 1.6 to 6.25 eV by employing different synthetic processes and post-treatments [55]. These features of $Ti_3C_2T_x$ MXene open new doors for its application as highly efficient ETL/HTL for PSCs application. The $Ti_3C_2T_x$ MXene can be prepared at low temperature, which makes it compatible with PSCs manufacturing technology.

In 2009, Kojima et al. proposed the novel PSCs using methyl ammonium lead iodide ($MAPbI_3$) as absorber layers [56]. The PCE of the proposed PSCs was less than 4%. Thus, various efforts have been made by various research groups to further improve the performance of the PSCs. The PSCs consist of various components such as an absorber layer, ETL, and HTL [44–46]. Titanium dioxide (TiO_2) has been widely used as ETL for the fabrication of PSCs, but suffers from the presence of trapping states [45]. Many attempts were also made to overcome such issues using novel electron transport materials. The $Ti_3C_2T_x$ MXene has excellent charge-carriers mobility and optoelectronic features, and can be utilized as ETL and HTL for the construction of PSCs. In addition, $Ti_3C_2T_x$ MXene also possesses excellent electrochemical properties, conductivity, and high surface area [57]. Thus, $Ti_3C_2T_x$ MXene has been used in the fabrication of various sensors and biosensors. In case of sensing-related applications, various enzymatic biosensors and non-biosensors have been reported using $Ti_3C_2T_x$ MXene-based electrode materials as electro-catalysts [57–60].

Herein, we have compiled and discussed the recent progress of $Ti_3C_2T_x$ MXene for the development of PSCs and electrochemical biosensors/non-biosensors applications. This review article would be beneficial for the scientific community working in the field of PSCs and electro-analytical sensing applications.

2. Synthetic Procedures for $Ti_3C_2T_x$ MXene

The $Ti_3C_2T_x$ MXene was discovered by Gogotsi and coworkers in 2011 [49]. The $Ti_3C_2T_x$ MXene was obtained by HF treatment followed by the sonication process, as depicted in Figure 1a–d. The SEM image of the synthesized $Ti_3C_2T_x$ MXene has been presented in Figure 1d, which demonstrates the presence of the layered structure of the prepared $Ti_3C_2T_x$ MXene. Yu et al. [61] also reported the synthesis of $Ti_3C_2T_x$ MXene. In brief, an appropriate amount of LiF was slowly added to the 9 molar HCl using stirring which yielded a homogeneous solution. In further steps, titanium aluminium carbide (Ti_3AlC_2) was milled by mortar and pestle and gradually mixed to the above-prepared homogeneous solution. This etching process was continued to 24 h at 25 °C using continuous stirring. Finally, the etched product was washed with DI water using centrifuge. This process was repeated for several times until the pH of the mixture reached above 6. Subsequently, handshaking was used to exfoliate the $Ti_3C_2T_x$ into the few-layer flakes. The dispersion of $Ti_3C_2T_x$ was degassed with Ar and stored in the fridge at 4 °C [61,62]. In 2019, Yang et al. [63] also reported the preparation of $Ti_3C_2T_x$. In the first step, Ti powder, aluminum powder, and graphite powder were mixed uniformly. This mixture was sintered at high temperature (1650 °C) for 2 h under Ar atmosphere to obtain the Ti_3AlC_2 (MAX phase). Then, Ti_3AlC_2 powder was grinded and added to the LiF/HCl mixture solution, and kept for the etching process for 24 h. After 24 h, the acidic mixture was centrifuged and washed with DI water until pH of the solution reached 6 and finally $Ti_3C_2T_x$ MXene was obtained [63]. The schematic illustration for the preparation of $Ti_3C_2T_x$ MXene is presented in Figure 1e. In the past few years, many synthetic procedures have been developed for the preparation of Ti_3C_2 MXene. In this section, we have briefly discussed two widely used and efficient etching and exfoliation synthetic procedures as given below.

2.1. Etching Method

A previous report showed that the MAX phase of the MXene can be chemically etched by using HF aqueous solution and the etching process can be described as below [64],

$$2Ti_3AlC_2 + 6HF \longrightarrow 2AlF_3 + 3H_2 + 2Ti_3C_2 \quad (1)$$

$$Ti_3C_2 + 2H_2O \longrightarrow Ti_3C_2 + Ti_3C_2(OH)_2 + H_2 \quad (2)$$

$$Ti_3C_2 + 2HF \longrightarrow Ti_3C_2F_2 + H_2 \quad (3)$$

The $Ti_3C_2T_x$ MXene can be prepared by the etching of Al from the Ti_3AlC_2 phase using HF as an etching agent. Studies have shown that H and F radicals broke down after being adsorbed onto Ti atoms, leading to the weakening of Al-Ti bonds. This resulted in the creation of surface terminals and, eventually, the formation of $Ti_3C_2T_x$ [64–66]. Because chemical etching operates under kinetic control, it is necessary to take into account various significant reaction factors such as time, temperature, and the concentration of HF. It was documented that achieving proper etching of a significant quantity in $M_{n+1}AX_n$ demands extended etching duration, a relatively elevated etching temperature, and a low pH level. The primary resulting compound during the etching process is AlF_3 (as shown in Equation (1)), which is insoluble in water. Hence, the careful selection of suitable temperature and duration is crucial to prevent the formation of AlF_3 precipitates. Moreover, the direct use of HF is very dangerous. Thus, to avoid the direct utilization of toxic HF, Halim and colleagues opted for a safer and less intense approach by using NH_4HF_2 instead of the hazardous HF for their etching process [67]. Similarly, Ghidiu et al. [68] took an alternative route by introducing Ti_3AlC_2 powder into a mixture of LiF and HCl (6 M) to produce $Ti_3C_2T_x$. They conducted the reaction at 40 °C for 45 h, and their findings highlighted that the presence of both fluorine ions and protons played a crucial role in the successful etching. Expanding on this method, Lipatov et al. [69] adjusted the ratios of MAX and LiF (MAX:

LiF = 1:5 or 1:7.5), revealing that an excess of LiF facilitated the etching of Al, along with the insertion of Li^+. As a result, $Ti_3C_2T_x$ MXene nanosheets were achieved, boasting larger dimensions, uniform thickness, and fewer imperfections. The etching procedure essentially converted the compact MAX structure into a loosely arranged, accordion-like configuration, recognized as multilayer MXenes (ML-MXenes). Consequently, a separate exfoliation step became essential to isolate the ML-MXenes into individual monolayers. It is important to mention that wet-chemical techniques are unsuitable for etching nitride-based MAXs because they have a higher energy barrier for formation. Urbankowski and colleagues [70] came up with an alternative approach involving molten salt (like potassium fluoride, lithium fluoride, and sodium fluoride) to create Ti_4N_3-based MXene. They achieved this by selectively removing aluminum from Ti_4AlN_3 at 550 °C in an argon environment. The leftover fluoride in the produced powder was subsequently eliminated using a solution of sulfuric acid (H_2SO_4).

2.2. Exfoliation Method

In 2013, the process of exfoliating MXene nanosheets into individual layers involved the introduction of large organic molecules into the spaces between the layers of the accordion-shaped structure [71]. This was followed by either mechanical vibration or the use of ultrasonic energy [72]. Common substances used to create these spaces, known as intercalants, included tetrabutylammonium hydroxide (TBAOH), dimethyl sulfoxide, hydrazine, urea, and NH_4^+ [73–76]. For instance, researchers led by Chia employed TBAOH as the intercalant to exfoliate $Ti_3C_2T_x$ MXene from products obtained through HF etching [59]. The process involved expanding the MAX powder containing larger flakes after removing Al. This resulted in Ti_3C_2-HF, which was then separated into individual or a small number of MXene layers by reducing the interaction between layers using TBAOH. Alternatively, when NH_4HF_2 was used as the etchant, the accordion-like multilayer $Ti_3C_2T_x$ MXene already contained cations like NH_4^+ within the aqueous solution.

2.3. Structural and Physiochemical Properties of $Ti_3C_2T_x$ MXene

The $Ti_3C_2T_x$ MXene consists of an interlayer region, intra-layer skeleton region, and surface terminating groups. The Ti and C atoms are stacked in the intra-molecular skeleton region to form the ionic bonds. In case of the interlayer region, the interaction between the layers was connected through the hydrogen bonding between either F/O atoms or van der Waals forces between O and F atoms. It was also observed that the strength of the hydrogen bonding depends not only on the number or distribution of –OH groups but also on the orientation of –OH. A large number of termination groups are also distributed on the $Ti_3C_2T_x$ MXene surface. The properties of the $Ti_3C_2T_x$ MXene can be influenced by the presence of functional groups. The $Ti_3C_2T_x$ MXene has good charge carrier mobility, metallic conductivity, and work function, which suggest its potential applications in photovoltaic devices. The transformation of the MAX phase to MXene phase has been illustrated in Figure 1a–c, whereas the scanning electron microscopic (SEM) picture of the MXene is presented in Figure 1d.

2.4. Charge Transport Properties of $Ti_3C_2T_x$ MXene

The $Ti_3C_2T_x$ MXene possesses excellent charge transport properties, which makes it suitable ETL and/or HTL materials for the fabrication of high-performance PSCs. Here are several essential facets related to its properties of charge transport. The $Ti_3C_2T_x$ MXene demonstrates excellent electrical conductivity, which is desirable and the most crucial feature for their applications in electronic devices. The presence of the metallic nature in $Ti_3C_2T_x$ MXene arises from its unique layered structure, which includes transition metal carbide layers that facilitate the effective charge transport [49].

In addition, delocalized electronic transition states in the $Ti_3C_2T_x$ MXene structure contribute to its presence of metallic properties. The presence of metallic Ti-C bonds in the $Ti_3C_2T_x$ MXene allows the movement of electrons and is responsible for the high conductiv-

ity of $Ti_3C_2T_x$ MXene. The charge carriers, such as electrons, experience the high mobility in the $Ti_3C_2T_x$ MXene and contribute to its excellent charge transport properties [77]. Thus, it is clear that high carrier mobility is crucial for electronic applications, as it can allow for efficient and fast movements of charge carriers. Due to the favorable charge transport properties, $Ti_3C_2T_x$ MXene can be used as efficient ETL or HTL for the development of PSCs [63].

It can be noted that research in the field of $Ti_3C_2T_x$ MXene is ongoing, and new findings may further uncover additional details regarding the charge transport properties.

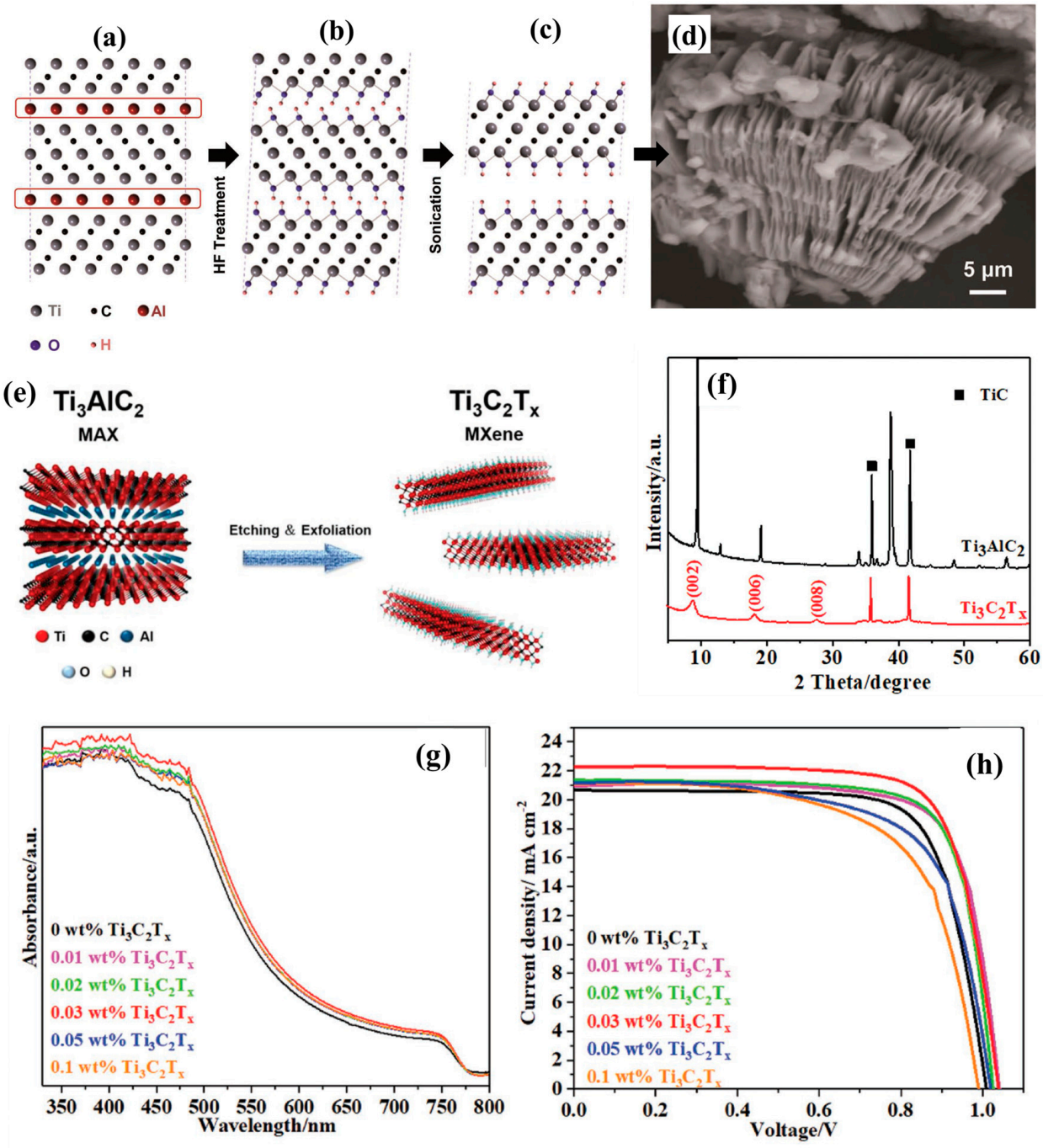

Figure 1. Schematic diagram (**a**–**c**) for the preparation of $Ti_3C_2T_x$ MXene and SEM image (**d**) [49]. Schematic illustration for the preparation of $Ti_3C_2T_x$ MXene (**e**) [63]. PXRD (**f**) of $Ti_3C_2T_x$ MXene. UV-vis spectra (**g**) and J-V curves (**h**) of the $Ti_3C_2T_x$/$MAPbI_3$ [77]. Reprinted with permissions from Refs. [49,63,77].

3. $Ti_3C_2T_x$ MXene in PSCs

3.1. $Ti_3C_2T_x$ MXene as Additive for PSCs

The $Ti_3C_2T_x$ MXene has excellent stability under ambient conditions and moisture. Perovskite materials are sensitive to the moisture and ambient conditions. Therefore, the use of $Ti_3C_2T_x$ MXene as additive to the perovskite material may significantly improve the stability of the perovskite materials. Hence, $Ti_3C_2T_x$ MXene can be used as additive for the development of highly stable PSCs. Therefore, Ma and his research team investigated the role of the synthesized $Ti_3C_2T_x$ MXene as an additive to control the crystallization of the absorber layer ($MAPbI_3$; where M = $CH_3NH_3^+$) for PSCs [77]. Authors used the acidic etching method for the preparation of $Ti_3C_2T_x$ MXene. The powder X-ray diffraction pattern (PXRD) of the $Ti_3C_2T_x$ MXene showed the well-defined diffraction peaks (Figure 1f) which confirmed the formation of the $Ti_3C_2T_x$ MXene phase. Further, authors developed PSCs using tin oxide (SnO_2) as an electron transport layer and introduced $Ti_3C_2T_x$ MXene as an additive to improve the charge transportation process. Authors introduced different weight percentages of $Ti_3C_2T_x$ to the SnO_2 layer and observed that the introduction of $Ti_3C_2T_x$ enhanced the optical properties of the SnO_2 layer (Figure 1g). The developed PSCs with $Ti_3C_2T_x$ as an additive exhibited the highest PCE of 16.80% (Figure 1h). This enhanced PCE may be due to the better electron transfer and lower charge transfer resistance.

In another report published in 2019, Agresti et al. [78] proposed novel strategies to tune the work function of the $Ti_3C_2T_x$ MXene. The PCE of $Ti_3C_2T_x$ MXene incorporated $MAPbI_3$-based PSCs, which can be further improved. In this work, authors investigated the critical role of $Ti_3C_2T_x$ MXene for work function tuning and interfacial engineering of PSCs. The $Ti_3C_2T_x$ MXene with different termination groups (T*x*) was employed to engineer the perovskite/electron transport layer interface and tune the work function of the perovskite light absorber and TiO_2 electron transport layer. Authors found that MXenes can efficiently tune the work function of perovskite light absorber and electron/hole transport layers without affecting other properties of the perovskite or electron transport layers. This showed the potential applications of MXene in the development of PSCs. However, the critical role of MXenes in the work function or interfacial engineering needs to be further investigated for various optoelectronic applications [79]. In other work, Zhang et al. [80] decorated $MAPbBr_3$ by few-layered $Ti_3C_2T_x$ sheets by employing the in situ solution growth method.

3.2. $Ti_3C_2T_x$ MXene as ETL for PSCs

Since efficient electron transportation is crucial for achieving high efficiency of the PSCs, ETL plays a vital role in the development of high-performance PSCs. The $Ti_3C_2T_x$ MXene has excellent properties such as high electrical conductivity, which is a desirable feature for an ETL. The ETL with high electrical conductivity provides the better electron transportation and reduces the electron recombination process. $Ti_3C_2T_x$ MXene has suitable electron affinity, which may be useful to collect and transport the electrons efficiently. The physiochemical properties of the $Ti_3C_2T_x$ MXene can be tuned or modified through surface functionalization or by incorporating it into composite materials. These features suggested that $Ti_3C_2T_x$ MXene may be used as ETL in the development of PSCs. The performance of the PSCs largely depends on the electron transport layer, perovskite light absorber layer, and hole transport layer. Hence, Chen et al. [81] developed $Ti_3C_2T_x$ quantum dots to engineer the perovskite/electron transport layer interface and an improved PCE of 21.64% was reported. Yang et al. [82] prepared a novel electron transport layer ($Ti_3C_2T_x/SnO_2$) to improve the photovoltaic performance of the PSCs. Ti_3C_2 MXene was prepared by etching of Ti_3AlC_2 as shown in Figure 2a. The developed PSCs using $Ti_3C_2T_x/SnO_2$ as an electron transport layer exhibited the enhanced PCE of 18.34%. The lowest PCE of 5.28% was achieved for the Ti_3C_2 MXene-based PSCs device, while a relatively high PCE of 17.23% was achieved for the SnO_2-based PSCs device. This showed that the presence of $Ti_3C_2T_x$ MXene enhanced the electron transportation and an improved PCE of 18.34% was achieved [82]. The energy level diagram of the $Ti_3C_2T_x/SnO_2$-based PSCs is

presented in Figure 3a. The incorporation of $Ti_3C_2T_x/SnO_2$ as an electron transport layer not only improves the charge extraction but also enhances the photovoltaic performance of the developed PSCs. Huang et al. [83] also developed a multi-dimensional conductive network (MDCN) electron transport layer using $Ti_3C_2T_x$ MXene for the construction of high-performance PSCs (Figure 2b). The enhanced PCE of 18.44% was reported for the MDCN-based PSCs device. Moreover, the developed PSCs device showed good stability in air for more than 45 days. Wang et al. [84] also developed a PSCs device using a $Ti_3C_2T_x$ MXene-modulated electrode/SnO_2 interface. The $Ti_3C_2T_x$ MXene was prepared by the chemical exfoliation method and employed as charge transport material. The energy level values of the $Ti_3C_2T_x$ MXene were found to be well suited with the energy level values of the SnO_2 (Figure 3b).

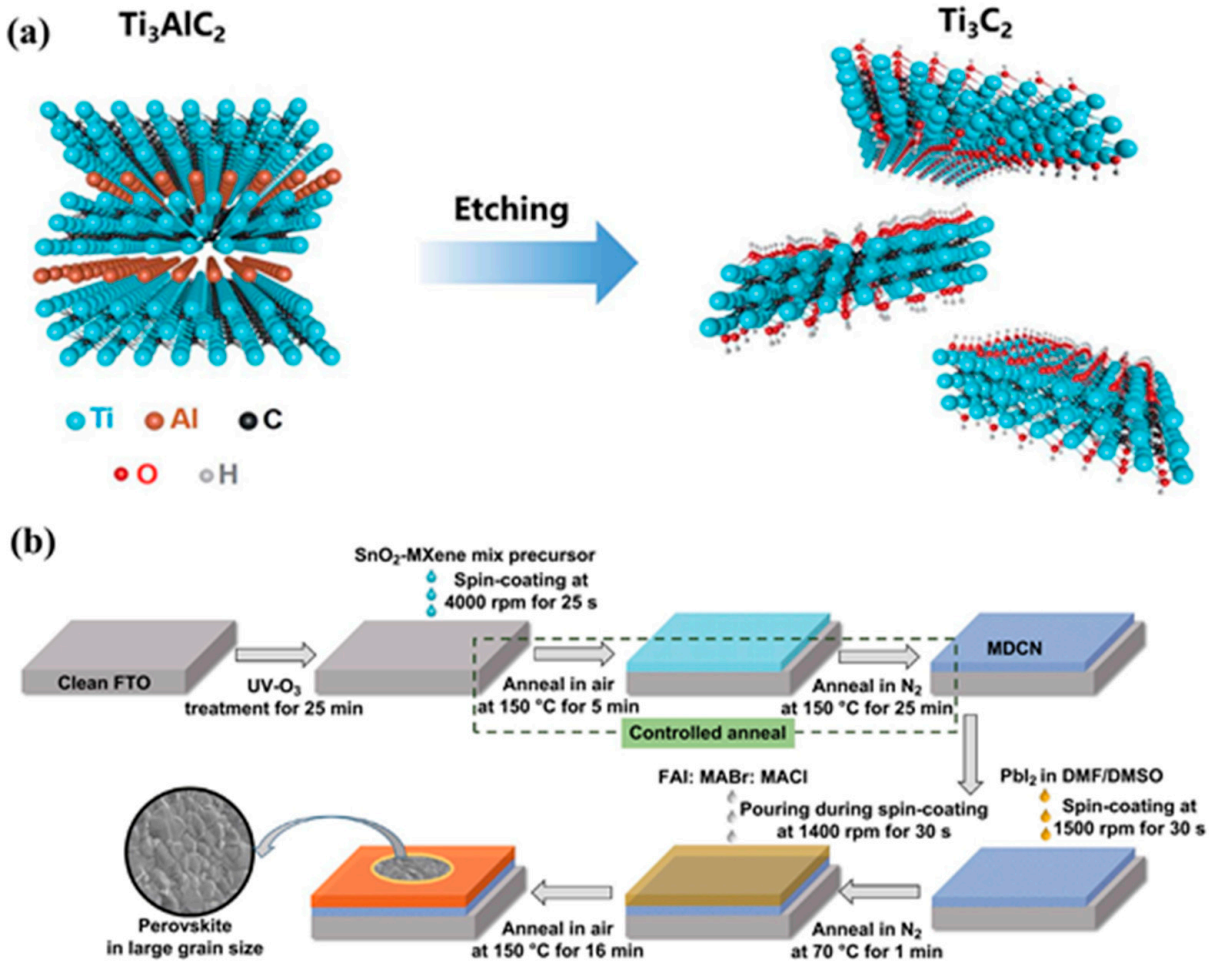

Figure 2. Schematic presentation for the preparation of MXene (**a**) and fabrication of PSCs (**b**). Reprinted with permission from Refs. [82,83].

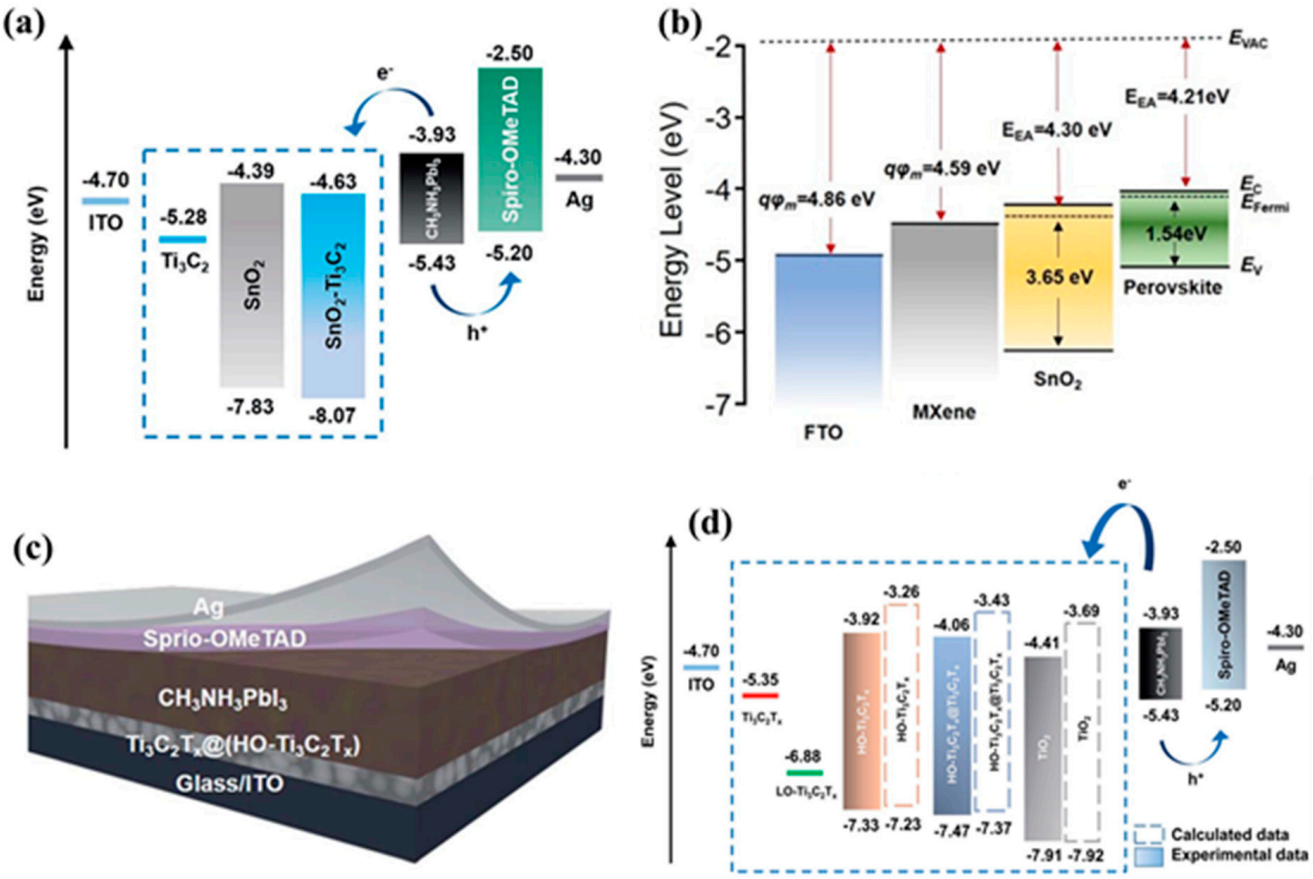

Figure 3. Energy level diagrams (**a**,**b**,**d**) and schematic diagram (**c**) of the MXene-based PSCs. Reprinted with permissions from Refs. [82,84,85].

The developed PSCs device exhibited a high PCE of 20.6% with good stability up to 3 months. The introduction of $Ti_3C_2T_x$ MXene enhanced the device stability as well as photovoltaic performance. This suggested the potential application of $Ti_3C_2T_x$ MXene in the development of PSCs. In 2021, Yang et al. [85] prepared $Ti_3C_2T_x$ MXene and investigated its properties for photovoltaic applications. The schematic picture of the developed PSCs is presented in Figure 3d. The energy level values of the $Ti_3C_2T_x$ MXene and other components have been summarized in Figure 3d. Authors found that energy level values of the $Ti_3C_2T_x$ MXene are well-matched with the energy values of the ITO and TiO_2. The developed PSCs using $Ti_3C_2T_x$ MXene showed the highest PCE of 18.29%. In other work, an interesting PCE of 15.71% was also obtained using $Ti_3C_2T_x$ MXene as dopant [86]. Yang et al. [63] developed the planar structured PSCs using $Ti_3C_2T_x$ MXene as an electron transport layer. The schematic diagram of the fabricated PSCs is depicted in Figure 4a. The cross-sectional SEM image of the developed PSCs is presented in Figure 4b, which is clearly showing the presence of interlayers. Yang et al. [63] investigated the effect of UV-ozone treatment. The observations showed that UV-ozone treatment slightly influenced the work function of the $Ti_3C_2T_x$ MXene (Figure 4c). The UV-ozone treatment enhanced the surface Ti-O bonds without affecting electron mobility, which suggested its potential use as an electron transport layer. The developed PSCs using $Ti_3C_2T_x$ MXene as an electron transport layer exhibited the excellent PCE of 17.17% [63]. In some other recent reports, Ge et al. [87] investigated the role of Ti_3C_2 quantum dots in PSCs and obtained the highest PCE of 16%.

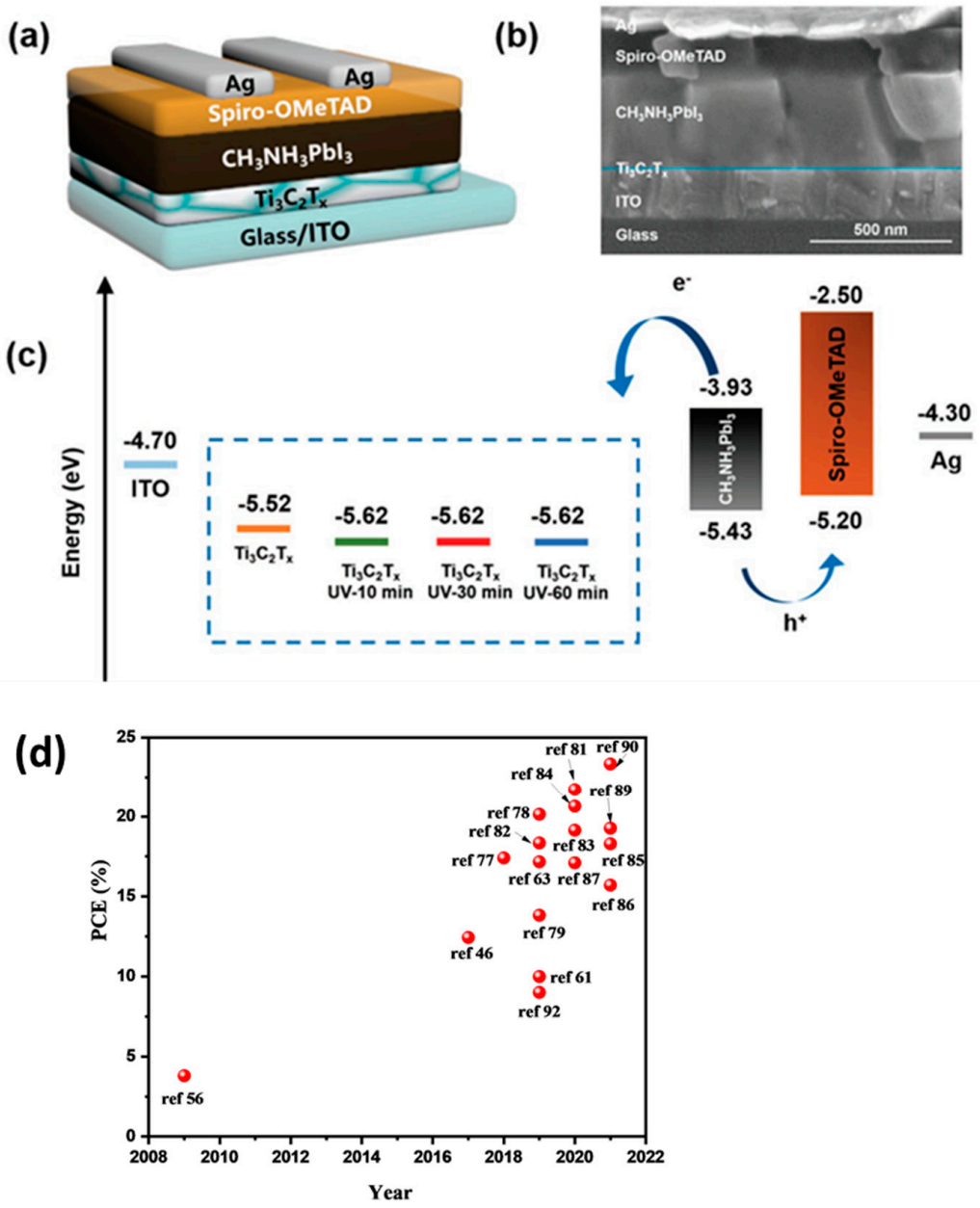

Figure 4. Schematic diagram (**a**), cross-sectional SEM (**b**) and energy level diagram (**c**) of the $Ti_3C_2T_x$ MXene-based PSCs. Reprinted with permissions from Ref. [63]. PCE (**d**) of previously published articles.

3.3. $Ti_3C_2T_x$ MXene as HTL for PSCs

The high conductivity of $Ti_3C_2T_x$ MXene may also be useful for its potential applications as HTL for the development of PSCs. The high conductivity $Ti_3C_2T_x$ MXene may facilitate the hole extraction and transportation, which alternatively improve the efficiency of the PSCs. Thus, $Ti_3C_2T_x$ MXene can be used as HTL for the development of PSCs. Cao et al. [79] also developed electrodes using 2D MXenes for the construction of HTL-free PSCs applications. The MXene-incorporated electrode-based PSCs exhibited the good PCE of 13.8% [79]. Saranin et al. [88] developed inverted p-i-n PSCs using $Ti_3C_2T_x$ MXene decorated with NiO and obtained a PCE of 19.2%. The recent progress in the enhancement of the PCE is depicted in Figure 4d. The above results showed that $Ti_3C_2T_x$ MXene has the potential for photovoltaic applications. The photovoltaic performances of the previously reported PSCs with $Ti_3C_2T_x$ MXene are summarized in Table 1.

Table 1. Photovoltaic performance of the recently reported PSCs.

S. No.	Device Structure	Voc (V)	Jsc (mA/cm^2)	FF	PCE (%)	References
1.	ITO/$Ti_3C_2T_x$/$CH_3NH_3PbI_3$/ Spiro-OMeTAD/Ag	1.08	22.63	0.70	17.17	[63]
2.	ITO/SnO_2/perovskite: $Ti_3C_2T_x$/Spiro-MeOTAD/Au	1.03	22.26	0.76	17.41	[77]
3.	FTO/c-TiO_2 +MXene/ m-TiO_2 + MXene/MXene/perovskite + MXene/ spiro-OMeTAD/Au	1.09	23.82	0.77	20.14	[78]
4.	FTO/TiO_2/$CH_3NH_3PbI_3$/ MXene	0.95	22.96	0.63	13.83	[79]
5.	c-TiO_2/m-TiO_2-TQD/perovskite/ Spiro-OMeTAD-$Cu_{1.8}S$	1.13	23.64	0.77	21.72	[81]
6	ITO/SnO_2-Ti_3C_2 MXene/$MAPbI_3$/Spiro-OMeTAD/ Ag	1.06	23.14	0.75	18.34	[82]
7.	FTO/SnO_2-MXene/ $(FAPbI_3)_{0.97}(MAPbBr_3)_{0.03}$/spiro-OMeTAD	1.07	24.52	0.77	19.14	[83]
8.	FTO/MXene-SnO_2/Perovskite/Spiro-OMeTAD/Au	1.11	24.34	-	20.65	[84]
9.	ITO/HO-$Ti_3C_2T_x$@$Ti_3C_2T_x$/$CH_3NH_3PbI_3$/ Spiro-OMeTAD/Ag	1.07	23.11	0.74	18.29	[85]
10.	ITO/SnO_2/$(BA)_2(MA)_4Pb_5I_{16}$-Ti_3C_2 MXene/Spiro-OMeTAD/Ag	1.11	20.87	0.67	15.71	[86]
11.	FTO/c-TiO_2/ m-TiO_2-2D MXene/ perovskite-0D Ti_3C_2 QDs/Spiro-OMeTAD/Au	0.92	19.6	0.66	17.1	[87]
12.	FTO/SnO_2/perovskite: $Ti_3C_2T_x$/Spiro-MeOTAD/Au	1.12	23.48	0.73	19.27	[89]
13.	ITO/SnO_2-MQDs/perovskite/ Spiro/MoO_3/Au	1.17	24.96	0.79	23.34	[90]
14.	FTO/$Ti_3C_2T_x$@TiO_2 (0.2 wt%)/$Cs_2AgBiBr_6$/Spiro/MoO_3/Ag	0.96	4.14	0.70	2.81	[91]
15.	FTO/TiO_2/$CsPbBr_3$/ Ti_3C_2-MXene/C	1.44	8.54	0.73	9.01	[92]
16.	FTO/c-TiO_2/$CsPbBr_3$/C+ CNTs+MXene	1.35	7.16	0.72	7.09	[93]

4. Electrochemical Sensing Applications

4.1. Electrochemical Properties of Ti_3C_2 MXene

The distinctive attributes of MXene (with Ti_3C_2 being the predominant variant) in contrast to other two-dimensional substances have led to its growing application in fabricating electrochemical sensors. These distinctive features can be outlined as follows.

MXene boasts a distinct benefit in terms of its high electrical conductivity, a crucial factor for enhancing the speed of electron transfer in heterogeneous reactions when compared to other 2D materials [94]. This exceptional conductivity characteristic forms a fundamental basis for its application in electrochemical sensors. The synthesis of MXene with favorable solution dispersibility and stability is straightforward. This is of paramount importance

for creating electrochemical sensors, given that the predominant technique for preparing modified electrodes involves pre-preparation of a well-dispersed coating solution for drop-casting. MXene serves as a robust material for substrate applications in printing scenarios. The methods of printing and pre/post-patterned coating offer an array of uncomplicated, economically viable, adaptable, and environment-friendly manufacturing methods for devices. Printing facilitates intricate 3D structures and multi-functional qualities, highly sought after in diverse applications. Hence, the introduction of MXene could propel printing/coating towards a more potent tool for fabricating devices and advancing industrial processes [95]. Leveraging its high stretch capacity and compatibility with living organisms, MXene stands as an excellent substrate choice for producing flexible conductive platforms. These platforms hold significant potential in crafting wearable electrochemical sensors, a pressing need for health monitoring and clinical analysis. With its two-dimensional layered structure and distinctive surface featuring numerous chemical groups, MXene displays considerable promise for integration with various functional materials or biomolecules for diverse analytical objectives. Various MXene-based nanostructures showcase a range of distinct and vibrant properties, offering opportunities for designing electrochemical sensors or devices with assorted functions, particularly in the realm of novel ECL or PEC sensors [96]. MXene's compatibility with biomolecules such as enzymes, proteins, and nucleic acids, coupled with its non-toxic nature, renders it as an excellent carrier in biosensors or biomedical applications. The exceptional photothermal conversion capability of MXene enables the realization of a dual-mode detection strategy in electrochemical sensor design. This expands the array of signal strategies available for electrochemical sensors, as evidenced by recent advancements in this field [97]. Herein, we have compiled recent works on the development of Ti_3C_2-based biosensors.

4.2. Ti_3C_2-Based Enzymatic Biosensors

The fundamental aspect of constructing electrochemical biosensors involves the essential direct transfer of electrons (DET) between enzymes and electrodes. MXene materials exhibit a range of unique characteristics, such as a high specific surface area and remarkable electrical conductivity [98]. Hence, the integration of MXene could potentially serve as an effective approach to promote the electron transfer process. The pioneering MXene in this context, namely Ti_3C_2, was employed in developing electrochemical sensors. Notably, the inaugural Ti_3C_2-based electrochemical sensor, crafted in 2014, was an enzyme-based biosensor, designed to detect H_2O_2 [99]. In this regard, Ti_3C_2 MXene was utilized for immobilizing the enzyme hemoglobin (Hb). This immobilization showcased not only proficient enzyme immobilization capabilities but also furnished an advantageous microenvironment for sustaining the activity and stability of the protein. Furthermore, it facilitated the direct transfer of electrons within Hb, underscoring the efficacy of anchoring enzymes onto the surface of Ti_3C_2 MXene as a means to produce mediator-free enzyme-centric biosensors. Endeavors were also undertaken to immobilize other enzymes, such as acetylcholinesterase (AChE) and tyrosinase, onto the surface of Ti_3C_2 MXene [100,101]. These endeavors highlighted that Ti_3C_2 MXene, with its expansive specific surface area, favorable biocompatibility, hydrophilic surface, and exceptional metallic conductivity, indeed stands as a promising choice for serving as an excellent platform for immobilizing enzymes in the construction of enzyme-based biosensors. To enhance the performance of enzyme-based biosensors, many researchers have employed a strategy involving the integration of Ti_3C_2 MXene with various functional materials, particularly diverse nanomaterials, to form composite structures. For instance, Wang et al. improved the Ti_3C_2 MXene by attaching TiO_2 nanoparticles (NPs), resulting in an increased surface area for protein adsorption and preservation of enzymatic stability and activity [102]. This modified Ti_3C_2 MXene was utilized to create a biosensor for Hb (hemoglobin), exhibiting superior detection capabilities for H_2O_2, with a limit of detection (LOD) of 14 nM, surpassing the performance of the TiO_2NP-free biosensor. Moreover, Rakhi et al. developed a glucose oxidase (GOx)-based biosensor by constructing a nanocomposite of Au/Ti_3C_2 MXene [103]. The integration

of Au NPs endowed the composite with distinctive electrocatalytic properties through synergistic effects. The resulting GOx/AuNPs/Ti_3C_2/Nafion/GCE biosensor showcased a relatively high amperometric sensitivity of 4.2 μA mM^{-1} cm^{-2} and an LOD of 5.9 μM for glucose detection. Similarly, Jiang et al. [104] employed an Ag@Ti_3C_2 nanocomposite as a carrier for AChE (acetylcholinesterase), fabricating a biosensor for malathion detection. In a separate study, Song et al. [105] developed an AChE-based biosensor for the identification of organophosphorus pesticide (OP) methamidophos. This biosensor was founded on a three-dimensional (3D) composite structure of MnO_2@Mn_3O_4/MXene/AuNPs, achieving a remarkably low LOD of 0.134 pM for methamidophos. In the realm of glucose biosensing, the enzymatic process of glucose oxidation generates a potentially harmful byproduct, H_2O_2 [57]. This byproduct, however, frequently hinders the effectiveness of GOx (glucose oxidase) in practical applications. In order to address this concern, Wu, M. et al. devised a novel solution [57]. They engineered a hybrid nanoreactor utilizing a combination of Ti_3C_2, poly-L-lysine (PLL), and glucose oxidase (GOx) (Figure 5a,b). This nanoreactor exhibited the capability to drive both the sequential reactions of glucose oxidation and the subsequent breakdown of H_2O_2.

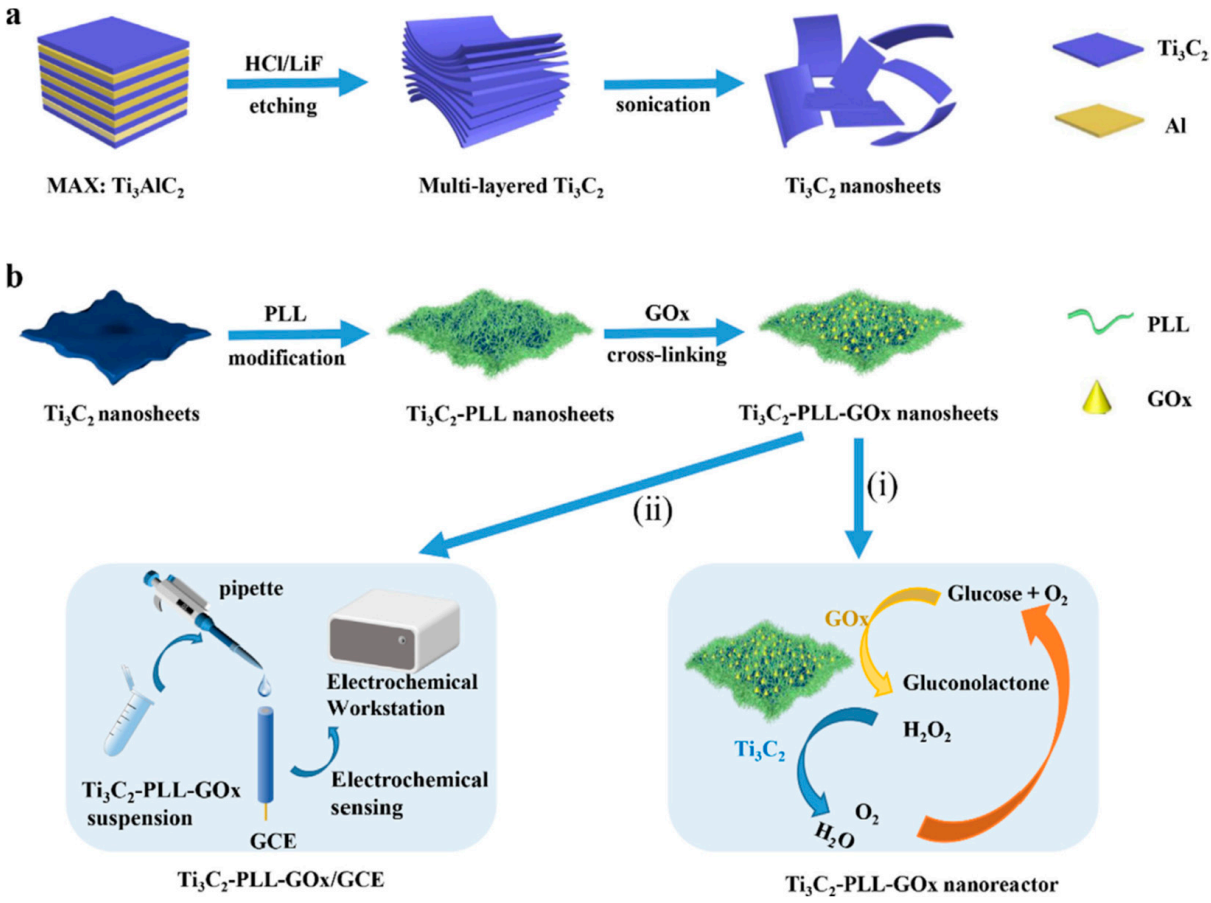

Figure 5. Schematic representation of the formation of the Ti_3C_2-PLL-GOx nanoreactor (**a**,**b**) and its application for cascade glucose oxidation (i) and electrochemical glucose sensing (ii) [57]. Reprinted with permission [57].

Interestingly, the Ti_3C_2 MXene component demonstrated proficiency in catalyzing the breakdown of H_2O_2. By incorporating GOx onto this platform, a cascading reaction for glucose oxidation was initiated. To realize this concept, the researchers fabricated Ti_3C_2/PLL/GOx nanoreactors, distinguished by their exceptional catalytic performance. These nanoreactors were then affixed to a glassy carbon electrode, creating a glucose biosensor with an impressive limit of detection (LOD) of 2.6 μM. Another notable advancement was accomplished by Wang et al. [106], who established a dual-enzyme biosensor for

inosine monophosphate (IMP) detection. In this approach, Ti_3C_2 MXene was combined with Au@Pt nanoflowers to harness robust catalytic abilities. Subsequently, two enzymes (5′-nucleotidase and xanthine oxidase) were immobilized on this composite. The resultant biosensor displayed an LOD of 2.73 ng/mL for inosine monophosphate detection in meat samples. The Ti_3C_2 MXene has the potential to serve as a constituent in conductive foundations within electrode arrangements beyond the glassy carbon electrode (GCE). Researchers created a composite called Ti_3C_2/graphene oxide (Ti_3C_2-GO), which was employed in crafting an inkjet-printed biosensor for hydrogen peroxide detection. This study revealed that the printable Ti_3C_2-GO composite exhibited remarkable capabilities as a sensing platform for electrochemical analysis [107]. Additionally, they developed a hybrid composite, Pt/PANI/MXene, by combining platinum particles, polyaniline, and Ti_3C_2 MXene [108]. This composite was utilized to modify a screen-printed carbon electrode (SPCE) to formulate a biosensor capable of detecting both hydrogen peroxide and lactate. The resulting SPCE demonstrated a low detection limit of 1.0 µM for H_2O_2. Following the immobilization of lactate oxidase, the biosensor facilitated lactate detection through amperometric measurements, achieving a detection limit of 5.0 µM for lactate. This biosensor proved its applicability for lactate measurement in milk samples, showcasing strong durability and dependability. The reported biosensors using Ti_3C_2 are compiled in Table 2.

Table 2. Sensing performance for enzymatic biosensors.

Materials	Sensing Analyte	Sensing Technique	Linear Range	LOD	References
Ti_3C_2	Glucose	CV	0.02–1.1; 4.0–20 mM	2.6 µM	[57]
Ti_3C_2	β-hydroxybutyrate	Amperometric	0.36–17.9 mM	45 µM	[58]
Ti_3C_2	Glucose	Amperometric	50–27,750 µM	23 µM	[59]
Ti_3C_2/Au-PdNPs	Paraoxon	Amperometric	0.1–1000 µg/L	1.75 ng/L	[60]

Zhao et al. [60] also fabricated a biosensor for the determination of pesticides. Figure 6 exhibits the fabrication of the biosensor. In this research, bimetallic nanoparticles consisting of a combination of gold and palladium (Au-Pd NPs) were synthesized through self-reduction occurring on the surface of ultrathin MXene nanosheets ($Ti_3C_2T_x$).

The resulting multi-dimensional nanocomposites (MXene/Au-Pd) demonstrate excellent conductivity and stability that prove advantageous for facilitating electron transfer and enzyme immobilization. By incorporating these nanocomposites into a disposable screen-printed electrode (SPE), a high-performance enzymatic biosensor was developed for swiftly detecting organophosphates (OPs). The electrochemical platform relies on the use of MXene/Au-Pd nanocomposites, as illustrated in Figure 6. The specific model pesticide chosen for this study was paraoxon, due to its high toxicity and the potential for its conversion from other OPs.

Figure 7a,b depict the Differential Pulse Voltammetry (DPV) outcomes of the SPE/MXene/Au-Pd under varying conditions: (a) diverse durations of Au-Pd NP growth, and (b) distinct ratios of Au^{3+} to Pd^{2+} concentrations, all conducted in a 0.1 M KCl solution containing 5.0 mM $K_3[Fe(CN)_6]$. In Figure 7a, the electric current response progressively rises until the 5-min mark, beyond which it declines. This decrease is possibly attributable to the congestion of NPs, which affects the kinetics of electron transfer. Evaluating both the morphology of the NPs and the DPV response, the researchers selected a growth period of 5 min as the optimal timeframe for Au-Pd NP formation. Additionally, the researchers fine-tuned the ratio of Au^{3+} to Pd^{2+} precursor concentrations. The most substantial DPV response occurs when the ratio stands at 1:2, as demonstrated in Figure 7b. Considering these findings, the researchers opted for the 1:2 concentration ratio for the Au^{3+}-Pd^{2+} precursor. The resultant sensor displayed commendable performance.

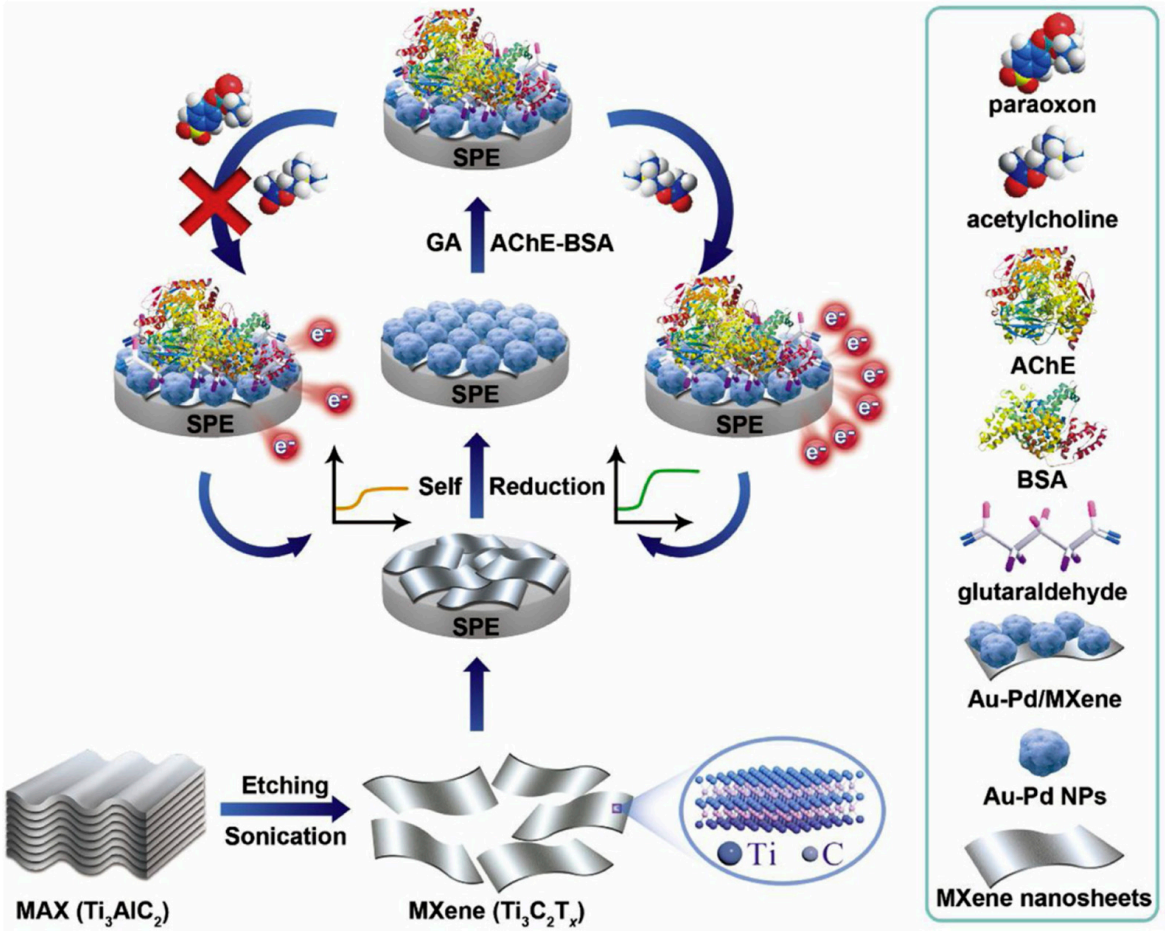

Figure 6. Schematic representation for the preparation of $Ti_3C_2T_x$ nanosheets and fabrication of enzyme-based pesticide biosensor ($Ti_3C_2T_x$/Au-Pd). Reprinted with permission [60].

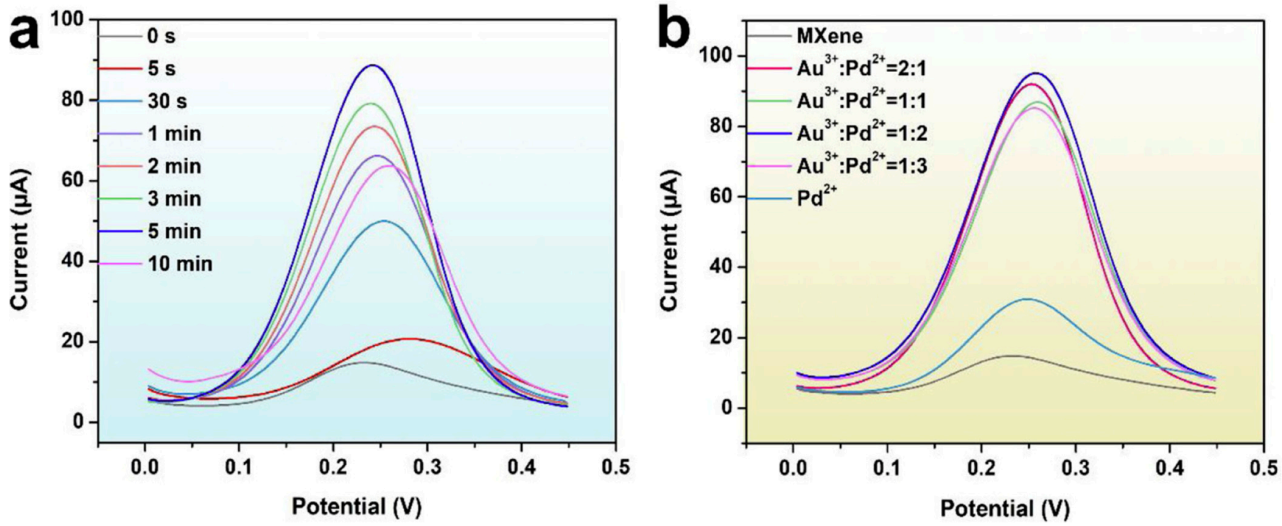

Figure 7. DPV response of SPE/MXene/Au-Pd with (**a**) different growth time of Au-Pd NPs and (**b**) different concentration ratios of Au^{3+} to Pd^{2+} in 0.1 M KCl solution containing 5.0 mM $K_3[Fe(CN)_6]$ [60]. Reprinted with permission [60].

4.3. Electrochemical Non-Biosensors

MXene could be utilized in creating electrochemical non-biosensors which do not require the immobilization of enzymes. In 2018, the initial electrochemical non-biosensor utilizing pristine Ti_3C_2 MXene was manufactured. This sensor was designed to detect the contaminant BrO_3^- in drinking water [109]. In this application, Ti_3C_2 MXene served as both a signal-enhancing matrix and a reducing agent, displaying remarkable electrocatalytic characteristics that facilitated effective reduction of BrO_3^-. Following this, two electrochemical sensors similar to the first one were developed using Ti_3C_2 MXene-modified glassy carbon electrodes (GCE). These sensors were used for the detection of the pesticide carbendazim [110] and the neurotransmitter dopamine [111]. In the case of carbendazim detection, the sensor achieved carbendazim redox at lower overpotentials compared to a graphene-based sensor [112]. The dopamine sensor demonstrated robust sensitivity, with a limit of detection (LOD) of around 3 nM for dopamine detection in actual samples. The incorporation of MXenes into other electrode systems, such as graphite composite paste electrodes (GCPE) [113] and screen-printed electrodes (SPE) [114], was also explored. An MXene/GCPE electrochemical sensor was devised for the detection of adrenaline. Notably, this was the first instance of introducing Ti_2C MXene into an electrochemical sensing system. The developed sensor achieved an LOD of 9.5 nM and could be further applied for detecting adrenaline in pharmaceutical samples, recovering between 99.2 and 100.8%. Another MXene-based electrochemical sensor was created using a screen-printed electrode (SPE) configuration for simultaneous voltammetric determination of acetaminophen (ACOP) and isoniazid (INZ). The Ti_3C_2 MXene displayed excellent electrocatalytic performance in the oxidation of ACOP and INZ compared to a bare SPE electrode in 0.1 M H_2SO_4. The distinct oxidation peak potentials allowed simultaneous detection of both targets. Consequently, this sensor attained LODs of 0.048 µM and 0.064 mM for ACOP and INZ, respectively. Additionally, the utilization of Ti_3C_2 MXene extended to the creation of various composites or combinations involving alternative substances or molecules, serving distinct analytical objectives. For instance, a hybrid of NiO and Ti_3C_2 was employed for detecting H_2O_2 without enzyme reliance [115]. Another example involves a three-dimensional porous composite of Ti_3C_2 and NiCo-LDH (Nickel-Cobalt layered double hydroxide) for glucose sensing without enzymes [116]. Furthermore, a composite of Au NPs and Ti_3C_2 was devised to sensitively detect nitrite [117]. A nanocomposite featuring Pd deposited on Ti_3C_2 was developed for swift, real-time detection of l-cysteine (l-Cys) [118]. A composite of $Mn_3(PO_4)_2$ and Ti_3C_2, synthesized using adenosine triphosphate (ATP) as a template, was applied for amperometric detection of superoxide anions $O_2^{\bullet -}$ released from HepG2 cells [119]. Another innovation involved a self-assembled nanocomposite of Ti_3C_2 and MWCNTs (multi-walled carbon nanotubes) for simultaneous electrochemical detection of hydroquinone (HQ) and catechol (CT) [120]. Moreover, a composite of methylene blue (MB), Cu NPs, and Ti_3C_2 was created for ratiometric electrochemical detection of piroxicam [121]. Throughout these studies, the performance of Ti_3C_2 MXene consistently proved highly effective in the design and operation of electrochemical sensors. The tendency of MXene to stack together is driven by hydrogen bonding and van der Waals interactions among its layers. This stacking can significantly reduce the effective surface area, thereby limiting its electrochemical performance. To counteract this issue, researchers like Tu et al. [122] introduced carbon nanohorns (CNHs) as spacers and created Ti_3C_2/CNHs nanocomposites. This layered MXene/CNHs structure displayed excellent conductivity, enhanced catalytic activity, and increased pathways for ion diffusion. Using this nanocomposite, they developed an electrochemical sensor for carbendazim with an impressive low detection limit of 1.0 nM. Similarly, Huang et al. [123] employed nitrogen-doped porous carbon derived from MOF-5-NH_2 (N-PC) as a spacer to prevent restacking of Ti_3C_2 MXene sheets, as shown in Figure 8.

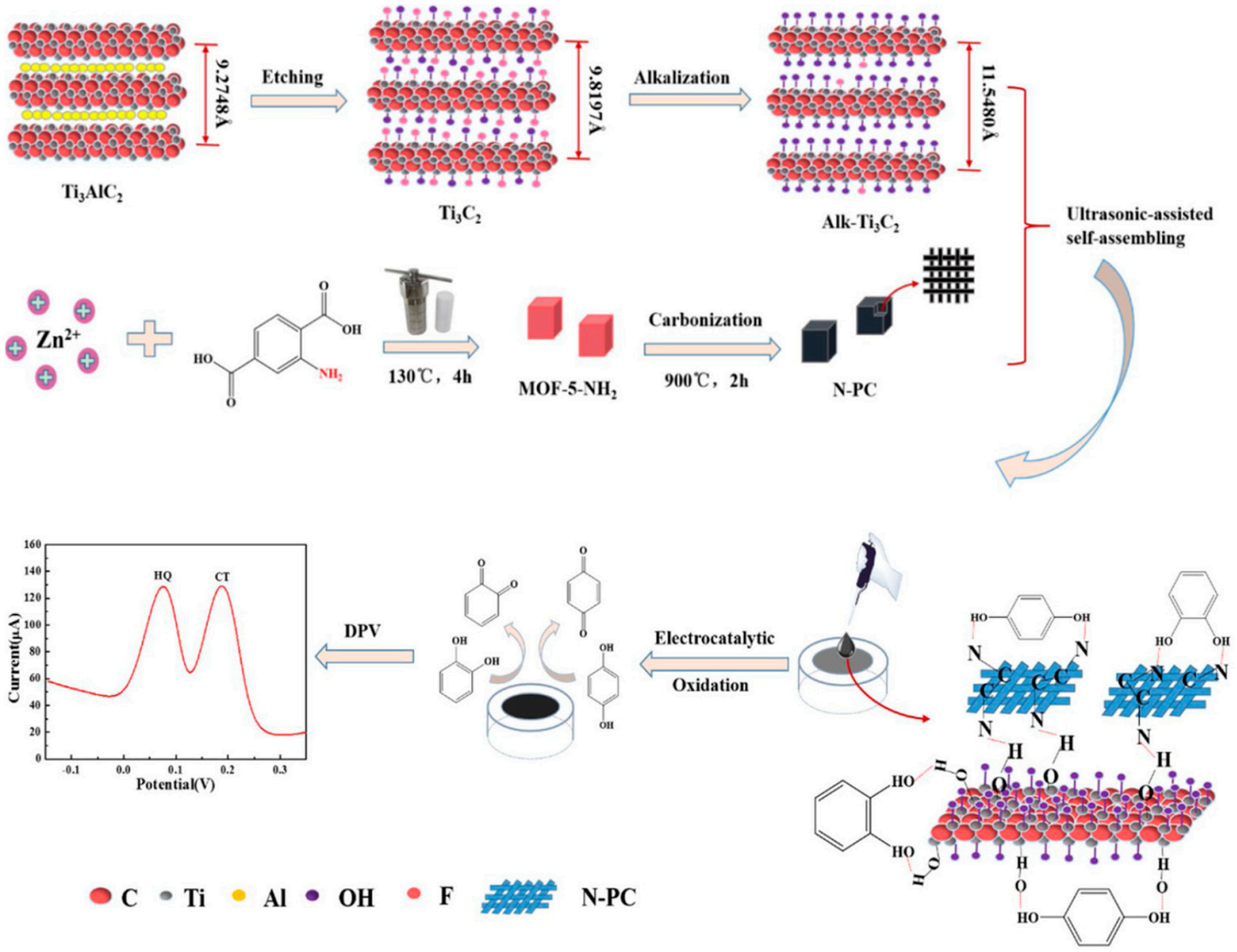

Figure 8. Schematic description of the preparation and application of alk-Ti_3C_2/N-PC/GCE [123]. Reprinted with permission [123].

Authors fabricated an alk-Ti_3C_2/N-PC electrochemical sensor for detecting hydroquinone (HQ) and catechol (CT) in industrial wastewater. In addition to using N-PC to prevent restacking, they treated the Ti_3C_2 MXene sheets with an alkaline intercalation process. This treatment led to the presence of abundant -OH groups on the MXene surface, which facilitated hydrogen-bond interactions for sensing HQ and CT. The resulting alk-Ti_3C_2/N-PC electrochemical sensor displayed low detection limits of 4.8 nM for HQ and 3.1 nM for CT, covering a broad linear range from 0.5 to 150 μM. Selectivity poses a challenge in the practical use of electrochemical sensors for targeted measurements. Molecularly imprinted polymers (MIPs) offer a solution to enhance sensor selectivity through specific recognition properties, cost-effectiveness, and quick synthesis. Ma et al. [124] developed a sensitive and selective electrochemical sensor for detecting fisetin using a hierarchical porous Ti_3C_2 MXene/amino carbon nanotubes (MXene/NH_2-CNTs) composite combined with MIP (Figure 9).

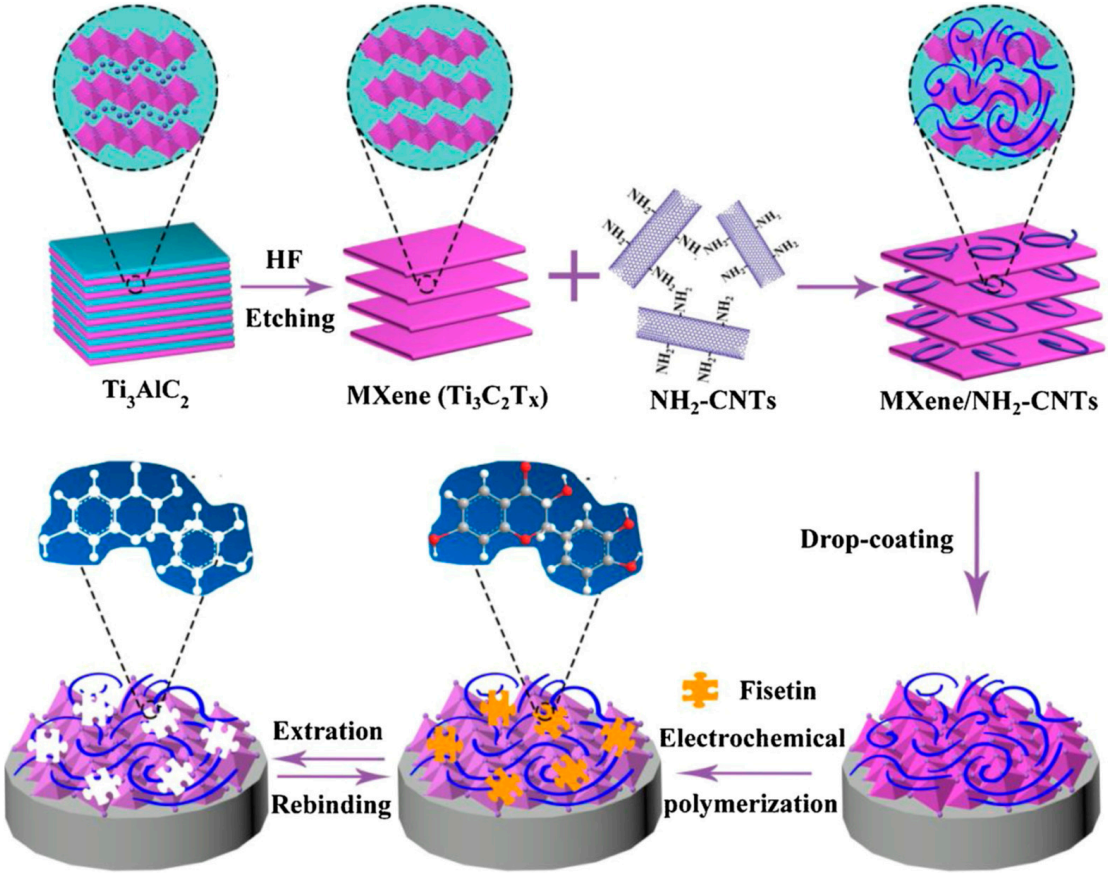

Figure 9. Schematic illustration for the preparation of MIP/MXene/NH_2-CNTs/GCE and the adsorption mechanism in the imprinted cavity [124]. Reprinted with permission [124].

The composite was formed by assembling negatively charged Ti_3C_2 flakes and positively charged NH_2-CNTs. The amino-functionalized CNTs not only provided good conductivity but also introduced positive charges on their surface, acting as spacers to prevent Ti_3C_2 MXene aggregation. The resultant MIP/Ti_3C_2 MXene/NH_2-CNTs/GCE sensor exhibited excellent analytical performance for fisetin detection, achieving a low LOD of 1.0 nM. Additionally, numerous advancements have been made in the field of electrochemical non-biosensors utilizing MXene-based materials. To facilitate the real-time and in situ detection of hydrogen peroxide (H_2O_2) released by living cells, Dang and colleagues [125] developed an electrochemical biosensor. This biosensor was constructed using titanium carbide (Ti_3C_2) nanosheets intercalated with Prussian blue nanoparticles (PB NPs/Ti_3C_2), achieving a notably low limit of detection (0.20 μM) for H_2O_2. Moreover, the PB NPs/Ti_3C_2 composite exhibited minimal harm to normal fibroblast cells across different time intervals and concentrations, underscoring its potential applicability in areas concerning living cells. In the realm of sulfadiazine detection, Kokulnathan et al. [126] synthesized nanocomposites of Ti_3C_2 and boron nitride (Ti_3C_2/BN) and designed an electrochemical catalytic sensor by modifying an electrode with Ti_3C_2/BN. This sensor exhibited a remarkably sensitive limit of detection (3.0 nM) for sulfadiazine. Kalambate and co-workers [127] developed an electrochemical sensor capable of detecting ifosfamide (IFO), acetaminophen (ACOP), domperidone (DOM), and sumatriptan (SUM). This sensor relied on a self-assembled nanocomposite thin film consisting of MXene, multi-walled carbon nanotubes (MWCNT), and chitosan. The limits of detection achieved for IFO, ACOP, DOM, and SUM were 0.00031, 0.00028, 0.00034, and 0.00042 μM, respectively. The reported sensors are summarized in Table 3.

Table 3. Sensing performance for non-biosensors.

Materials	Sensing Analyte	Sensing Technique	Linear Range	LOD	References
Ti_3C_2/PBNPs	Hydroquinone (HQ)	DPV	-	4.8 nM	[123]
Ti_3C_2/PBNPs	Catechol (CT)	DPV	0.5–150 μM	3.1 nM	[123]
Ti_3C_2/NH_2-CNTs	Fisetin	DPV	0.003–20.0 μM	1 nM	[124]
Ti_3C_2/BN	Sulfadiazine	DPV	0.01–44; 59–186 μM	3 nM	[126]
Ti_3C_2/MWCNT	Ifosfamide (IFO)	Adsorptive Stripping	0.0011–1.0 μM	0.00031 μM	[127]
Ti_3C_2/AuNPs	Folic acid (FA)	Amperometric	0.02–3580 μM	6.2 nM	[128]
Ti_3C_2/AuNPs	Uric acid (UA)	Amperometric	0.03–1520 μM	11.5 nM	[128]
Ti_3C_2/TiO_2	NO_2^-	DPV	0.003–0.25 mM	850 nM	[129]
Ti_3C_2/BiNPs	Pb^{2+}	SWV	0.06–0.6 μM	10.8 nM	[130]
Ti_3C_2/ZIF-8	Hydrazine	Amperometric	10 μm to 7.7 mM	5100	[131]

5. Conclusions and Future Perspective

MXenes, especially $Ti_3C_2T_x$ MXene, possess unique optoelectronic properties, and an adjustable composition/structure. The $Ti_3C_2T_x$ MXene is one of the most important 2D materials which has been used in various applications. The work function of the $Ti_3C_2T_x$ MXene can be easily tuned, which makes it the most suitable candidate as an electron and hole transport layer for perovskite solar cells. In the last 3–4 years, $Ti_3C_2T_x$ MXene has been used as an additive, electron/hole transport layers, and electrode materials for the development of perovskite solar cells. The reported literature showed that the incorporation of $Ti_3C_2T_x$ MXene not only enhances the photovoltaic performance of the perovskite solar cells but also improves long term stability. Therefore, it is clear that it would be beneficial to develop the novel device architectures of the perovskite solar cells with $Ti_3C_2T_x$ MXene-assisted metal oxide as an electron transport layer. This may improve the photovoltaic performance as well as long term stability of the perovskite solar cells. In the realm of future applications of MXene in electrochemical sensors, there are several potential research avenues. Firstly, in the context of biosensors, MXene is often utilized as a carrier for biomolecules. The common methods for immobilizing biomolecules on MXene surfaces involve the assistance of Au nanoparticles or electrostatic adsorption. However, we believe that establishing a direct chemical linkage between biomolecules and MXene holds greater value due to the enhanced stability of resulting biocomposites and the rich surface chemistry of MXene. This underscores the significance of surface functionalization techniques like amination or carboxylation of MXene. Further exploration of diverse combinations in this regard is warranted. In summary, leveraging MXene as a powerful tool opens up the possibility of developing more advanced electrochemical sensors in the future.

Author Contributions: Conceptualization, K.A. and A.C.; writing—original draft preparation, T.N. and A.C.; writing—review and editing, A.C. and H.K. All authors have read and agreed to the published version of the manuscript.

Funding: This research received no external funding.

Data Availability Statement: No new data were created, or where data is unavailable due to privacy or ethical restrictions.

Conflicts of Interest: The authors declare no conflict of interest.

References

1. Li, D.; Huang, Y.; Ma, R.; Liu, H.; Liang, Q.; Han, Y.; Ren, Z.; Liu, K.; Wai-Keung Fong, P.; Zhang, Z.; et al. Surface Regulation with Polymerized Small Molecular Acceptor Towards Efficient Inverted Perovskite Solar Cells. *Adv. Energy Mater.* **2023**, *13*, 2204247. [CrossRef]
2. Raza, W.; Ahmad, K. Visible Light-Driven Photocatalysts for Environmental Applications Based on Graphitic Carbon Nitride. In *Handbook of Nanomaterials and Nanocomposites for Energy and Environmental Applications*; Kharissova, O., Martínez, L., Kharisov, B., Eds.; Springer: Cham, Switzerland, 2020. [CrossRef]
3. Ahmad, K.; Chaudhary, A.; Raza, W.; Alsulmi, A.; Kim, H. Fabrication of MnO_2/g-C_3N_4 hetero-junction for hydrogen production and rhodamine B/methylene blue dye degradation. *Opt. Mater.* **2023**, *140*, 113857. [CrossRef]
4. Raza, W.; Ahmad, K.; Kim, H. Nitrogen-doped graphene as an efficient metal-free catalyst for ammonia and non-enzymatic glucose sensing. *J. Phys. Chem. Solids* **2022**, *160*, 110359. [CrossRef]
5. Ahmad, K.; Khan, M.Q.; Alsalme, A.; Kim, H. Sulfur-doped graphitic-carbon nitride (S@g-C_3N_4) as bi-functional catalysts for hydrazine sensing and hydrogen production applications. *Synth. Met.* **2022**, *288*, 117100. [CrossRef]
6. Mohammad, A.; Ansari, S.N.; Chaudhary, A.; Ahmad, K.; Rajak, R.; Tauqeer, M.; Mobin, S.M. Enthralling Adsorption of Different Dye and Metal Contaminants from Aqueous Systems by Cobalt/Cobalt Oxide Nanocomposites Derived from Single-Source Molecular Precursors. *ChemistrySelect* **2018**, *3*, 5733. [CrossRef]
7. Ahmad, K.; Kumar, P.; Shrivastava, P.; Mobin, S.M. Sn(IV) Inserted Lead-Free Perovskite Materials ($MA_3(Bi_{1-}xSn_x)_2I_9$) as Light Absorbers: Bandgap Engineering and Enhanced Photovoltaic Performance. *Energy Technol.* **2022**, *10*, 2100717. [CrossRef]
8. Kumar, P.; Ahmad, K.; Dagar, J.; Unger, E.; Mobin, S.M. Two-Step Deposition Approach for Lead Free $(NH_4)_3Sb_2I_9$ Perovskite Solar Cells with Enhanced Open Circuit Voltage and Performance. *ChemElectroChem* **2021**, *8*, 3150. [CrossRef]
9. Ahmad, K.; Shinde, M.A.; Kim, H. Molybdenum disulfide/reduced graphene oxide: Progress in synthesis and electro-catalytic properties for electrochemical sensing and dye sensitized solar cells. *Microchem. J.* **2021**, *169*, 106583. [CrossRef]
10. Ahmad, K.; Kim, H. Improved photovoltaic performance and stability of perovskite solar cells with device structure of (ITO/SnO_2/$CH_3NH_3PbI_3$/rGO+spiro-MeOTAD/Au). *Mater. Sci. Eng. B* **2023**, *289*, 116227. [CrossRef]
11. Ahmad, K.; Kim, H. Enhanced stability of $MAPbI_3$ based perovskite solar cells. *Mater. Lett.* **2022**, *318*, 132187. [CrossRef]
12. Ahmad, K.; Khan, M.Q.; Khan, R.A.; Kim, H. Numerical simulation and fabrication of Pb-free perovskite solar cells (FTO/TiO_2/$Cs_3Bi_2I_9$/spiro-MeOTAD/Au). *Opt. Mater.* **2022**, *128*, 112458. [CrossRef]
13. Ahmad, K.; Khan, M.Q.; Kim, H. Simulation and fabrication of all-inorganic antimony halide perovskite-like material based Pb-free perovskite solar cells. *Opt. Mater.* **2022**, *128*, 112374. [CrossRef]
14. Ding, Y.; Guo, Q.; Geng, Y.; Dai, Z.; Wang, Z.; Chen, Z.; Guo, Q.; Zheng, Z.; Li, Y.; Zhou, E. A low-cost hole transport layer enables $CsPbI_2Br$ single-junction and tandem perovskite solar cells with record efficiencies of 17.8% and 21.4%. *Nano Today* **2022**, *46*, 101586. [CrossRef]
15. Chen, J.; Dong, H.; Li, J.; Zhu, X.; Xu, J.; Pan, F.; Xu, R.; Xi, J.; Jiao, B.; Hou, X.; et al. Solar Cell Efficiency Exceeding 25% through Rb-Based Perovskitoid Scaffold Stabilizing the Buried Perovskite Surface. *ACS Energy Lett.* **2022**, *7*, 3685–3694. [CrossRef]
16. Ma, R.; Jiang, X.; Fu, J.; Zhu, T.; Yan, C.; Wu, K.; Müller-Buschbaum, P.; Li, G. Revealing the underlying solvent effect on film morphology in high-efficiency organic solar cells through combined ex situ and in situ observations. *Energy Environ. Sci.* **2023**, *16*, 2316–2326. [CrossRef]
17. Chen, B.; Chen, H.; Hou, Y.; Xu, J.; Teale, S.; Bertens, K.; Chen, H.; Proppe, A.; Zhou, Q.; Yu, D.; et al. Passivation of the Buried Interface via Preferential Crystallization of 2D Perovskite on Metal Oxide Transport Layers. *Adv. Mater.* **2021**, *33*, 2103394. [CrossRef]
18. Kumar, P.; Wu, F.Y.; Hu, L.H.; Abbas, S.A.; Ming, J.; Lin, C.N.; Fang, J.; Chu, C.W.; Li, L.J. High-performance graphene/sulphur electrodes for flexible Li-ion batteries using the low-temperature spraying method. *Nanoscale* **2015**, *7*, 8093–8100. [CrossRef]
19. Li, H.N.; Shi, Y.M.; Chiu, M.H.; Li, L.J. Emerging energy applications of two-dimensional layered transition metal dichalcogenides. *Nano Energy* **2015**, *18*, 293–305. [CrossRef]
20. Chhowalla, M.; Shin, H.S.; Eda, G.; Li, L.J.; Loh, K.P.; Zhang, H. The chemistry of two-dimensional layered transition metal dichalcogenide nanosheets. *Nat Chem.* **2013**, *5*, 263–275. [CrossRef] [PubMed]
21. Stephenson, T.; Li, Z.; Olsen, B.; Mitlin, D. Lithium ion battery applications of molybdenum disulfide (MoS_2) nanocomposites. *Energy Environ. Sci.* **2014**, *7*, 209.
22. Sun, G.Z.; Zhang, X.; Lin, R.Z.; Yang, J.; Zhang, H.; Chen, P. Hybrid Fibers Made of Molybdenum Disulfide, Reduced Graphene Oxide, and Multi-Walled Carbon Nanotubes for Solid-State, Flexible, Asymmetric Supercapacitors. *Angew. Chem. Int. Ed.* **2015**, *54*, 4651–4656. [CrossRef]
23. Yin, Z.Y.; Chen, B.; Bosman, M.; Cao, X.H.; Chen, J.Z.; Zheng, B.; Zhang, H. Au Nanoparticle-Modified MoS_2 Nanosheet-Based Photoelectrochemical Cells for Water Splitting. *Small* **2014**, *10*, 3537–3543. [CrossRef]
24. Wang, Q.H.; Kalantar-Zadeh, K.; Kis, A.; Coleman, J.N.; Strano, M.S. Electronics and optoelectronics of two-dimensional transition metal dichalcogenides. *Nat. Nanotechnol.* **2012**, *7*, 699–712. [CrossRef] [PubMed]
25. Ahmad, K.; Shinde, M.A.; Song, G.; Kim, H. Fabrication of MoS2/rGO/AgNWs on PET substrate for flexible electrochromic devices. *Synth. Met.* **2022**, *287*, 117074. [CrossRef]
26. Naguib, M.; Mochalin, V.N.; Barsoum, M.W.; Gogotsi, Y. 25th Anniversary Article: MXenes: A New Family of Two-Dimensional Materials. *Adv. Mater.* **2014**, *26*, 992–1005. [CrossRef] [PubMed]

27. Zheng, J.; Zhang, H.; Dong, S.H.; Liu, Y.P.; Nai, C.T.; Shin, H.S.; Jeong, H.Y.; Liu, B.; Loh, K.P. High yield exfoliation of two-dimensional chalcogenides using sodium naphthalenide. *Nat. Commun.* **2014**, *5*, 2995. [CrossRef]
28. Chang, Y.H.; Lin, C.T.; Chen, T.Y.; Hsu, C.L.; Lee, Y.H.; Zhang, W.J.; Wei, K.H.; Li, L.J. Highly Efficient Electrocatalytic Hydrogen Production by MoS_x Grown on Graphene-Protected 3D Ni Foams. *Adv. Mater.* **2013**, *25*, 756–760. [CrossRef] [PubMed]
29. Cao, X.H.; Shi, Y.M.; Shi, W.H.; Rui, X.H.; Yan, Q.Y.; Kong, J.; Zhang, H. Preparation of MoS_2-Coated Three-Dimensional Graphene Networks for High-Performance Anode Material in Lithium-Ion Batteries. *Small* **2013**, *9*, 3433–3438. [CrossRef] [PubMed]
30. Li, Y.G.; Wang, H.L.; Xie, L.M.; Liang, Y.Y.; Hong, G.S.; Dai, H.J. MoS_2 Nanoparticles Grown on Graphene: An Advanced Catalyst for the Hydrogen Evolution Reaction. *J. Am. Chem. Soc.* **2011**, *133*, 7296–7299. [CrossRef] [PubMed]
31. Eames, C.; Islam, M.S. Ion Intercalation into Two-Dimensional Transition-Metal Carbides: Global Screening for New High-Capacity Battery Materials. *J. Am. Chem. Soc.* **2014**, *136*, 16270–16276. [CrossRef]
32. Chen, J.Z.; Wu, X.J.; Yin, L.S.; Li, B.; Hong, X.; Fan, Z.X.; Chen, B.; Xue, C.; Zhang, H. One-pot synthesis of CdS nanocrystals hybridized with single-layer transition-metal dichalcogenide nanosheets for efficient photocatalytic hydrogen evolution. *Angew. Chem. Int. Ed.* **2015**, *54*, 1210–1214. [CrossRef]
33. Naguib, M.; Mashtalir, O.; Carle, J.; Presser, V.; Lu, J.; Hultman, L.; Gogotsi, Y.; Barsoum, M.W. Two-Dimensional Transition Metal Carbides. *Acs Nano* **2012**, *6*, 1322–1331. [CrossRef] [PubMed]
34. Ma, C.B.; Qi, X.Y.; Chen, B.; Bao, S.Y.; Yin, Z.Y.; Wu, X.J.; Luo, Z.M.; Wei, J.; Zhang, H.L.; Zhang, H. MoS_2 nanoflower-decorated reduced graphene oxide paper for high-performance hydrogen evolution reaction. *Nanoscale* **2014**, *6*, 5624–5629. [CrossRef]
35. Xie, Y.; Naguib, M.; Mochalin, V.N.; Barsoum, M.W.; Gogotsi, Y.; Yu, X.Q.; Nam, K.W.; Yang, X.Q.; Kolesnikov, A.I.; Kent, P.R.C. Role of Surface Structure on Li-Ion Energy Storage Capacity of Two-Dimensional Transition-Metal Carbides. *J. Am. Chem. Soc.* **2014**, *136*, 6385–6394. [CrossRef] [PubMed]
36. Raza, W.; Ahmad, K.; Kim, H. Fabrication of defective graphene oxide for efficient hydrogen production and enhanced 4-nitrophenol reduction. *Nanotechnology* **2021**, *32*, 495404. [CrossRef]
37. Ahmad, K.; Mobin, S.M. Graphene oxide based planar heterojunction perovskite solar cell under ambient condition. *New J. Chem.* **2017**, *41*, 14253–14258. [CrossRef]
38. Inamuddin Ahmad, K.; Naushad, M. Optimization of glassy carbon electrode based graphene/ferritin/glucose oxidase bioanode for biofuel cell applications. *Int. J. Hydrogen Energy* **2014**, *39*, 7417–7421. [CrossRef]
39. Ahmad, K.; Kumar, P.; Mobin, S.M. A highly sensitive and selective hydroquinone sensor based on a newly designed N-rGO/$SrZrO_3$ composite. *Nanoscale Adv.* **2020**, *2*, 502–511. [CrossRef]
40. Mohammad, A.; Ahmad, K.; Rajak, R.; Mobin, S.M. Binder Free Modification of Glassy Carbon Electrode by Employing Reduced Graphene Oxide/ZnO Composite for Voltammetric Determination of Certain Nitroaromatics. *Electroanalysis* **2017**, *30*, 274–282. [CrossRef]
41. Ahmad, K.; Mohammad, A.; Ansari, S.N.; Mobin, S.M. Construction of graphene oxide sheets based modified glassy carbon electrode (GO/GCE) for the highly sensitive detection of nitrobenzene. *Mater. Res. Express* **2018**, *5*, 078005. [CrossRef]
42. Ahmad, K.; Mohammad, A.; Mathur, P.; Mobin, S.M. Preparation of $SrTiO_3$ perovskite decorated rGO and electrochemical detection of nitroaromatics. *Electrochim. Acta* **2016**, *215*, 435–446. [CrossRef]
43. Le, Q.; Nguyen, T.; Jang, H.; Kim, S. The use of UV/ozone-treated MoS_2 nanosheets for extended air stability in organic photovoltaic cells. *Phys. Chem. Chem. Phys.* **2014**, *16*, 13123. [CrossRef] [PubMed]
44. Zhao, X.; Liu, S.; Zhang, H.; Chang, S.-Y.; Huang, W.; Zhu, B.; Shen, Y.; Shen, C.; Wang, D.; Yang, Y.; et al. 20% Efficient Perovskite Solar Cells with 2D Electron Transporting Layer. *Adv. Funct. Mater.* **2019**, *29*, 1805168. [CrossRef]
45. Tang, G.; You, P.; Tai, Q.; Yang, A.; Cao, J.; Zheng, F.; Zhou, Z.; Zhao, J.; Chan, P.K.L.; Yan, F. Solution-Phase Epitaxial Growth of Perovskite Films on 2D Material Flakes for High-Performance Solar Cells. *Adv. Mater.* **2019**, *31*, 1807689. [CrossRef]
46. Huang, P.; Wang, Z.; Liu, Y.; Zhang, K.; Yuan, L.; Zhou, Y.; Song, B.; Li, Y. Water-Soluble 2D Transition Metal Dichalcogenides as the Hole-Transport Layer for Highly Efficient and Stable p–i–n Perovskite Solar Cells. *ACS Appl. Mater. Interfaces* **2017**, *9*, 25323. [CrossRef] [PubMed]
47. Yin, G.; Zhao, H.; Feng, J.; Sun, J.; Yan, J.; Liu, Z.; Lin, S.; Liu, S. Low-temperature and facile solution-processed two-dimensional TiS_2 as an effective electron transport layer for UV-stable planar perovskite solar cells. *J. Mater. Chem. A* **2018**, *6*, 9132. [CrossRef]
48. Zhao, E.; Gao, L.; Yang, S.; Wang, L.; Cao, J.; Ma, T. In situ fabrication of 2D SnS_2 nanosheets as a new electron transport layer for perovskite solar cells. *Nano Res.* **2018**, *11*, 5913. [CrossRef]
49. Naguib, M.; Kurtoglu, M.; Presser, V.; Lu, J.; Niu, J.; Heon, M.; Hultman, L.; Gogotsi, Y.; Barsoum, M.W. Two dimensional nanocrystals produced by exfoliation of Ti_3AlC_2. *Adv. Mater.* **2011**, *23*, 4248–4253. [CrossRef] [PubMed]
50. Ren, A.; Zou, J.; Lai, H.; Huang, Y.; Yuan, L.; Xu, H.; Shen, K.; Wang, H.; Wei, S.; Wang, Y.; et al. Direct laser-patterned MXene-perovskite image sensor arrays for visible-near infrared photodetection. *Mater. Horiz.* **2020**, *7*, 1901–1911. [CrossRef]
51. Zhang, S.; Ying, H.; Yuan, B.; Hu, R.; Han, W.-Q. Partial atomic tin nanocomplex pillared few-layered $Ti_3C_2T_x$ MXenes for superior lithium-ion storage. *Nano-Micro Lett.* **2020**, *12*, 78. [CrossRef]
52. Lei, Y.; Zhao, W.; Zhang, Y.; Jiang, Q.; He, J.H.; Baeumner, A.J.; Wolfbeis, O.S.; Wang, Z.L.; Salama, K.N.; Alshareef, H.N. A MXene-based wearable biosensor system for high-performance in vitro perspiration analysis. *Small* **2019**, *15*, 1901190. [CrossRef]
53. Zhao, S.; Zhang, H.B.; Luo, J.Q.; Wang, Q.W.; Xu, B.; Hong, S.; Yu, Z.Z. Highly electrically conductive three-dimensional $Ti_3C_2T_x$ MXene/reduced graphene oxide hybrid aerogels with excellent electromagnetic interference shielding performances. *ACS Nano* **2018**, *12*, 11193–11202. [CrossRef] [PubMed]

54. Xu, M.; Lei, S.; Qi, J.; Dou, Q.; Liu, L.; Lu, Y.; Huang, Q.; Shi, S.; Yan, X. Opening magnesium storage capability of two-dimensional MXene by intercalation of cationic surfactant. *ACS Nano* **2018**, *12*, 3733–3740. [CrossRef] [PubMed]
55. Chen, C.; Wang, J.; Liu, D.; Yang, C.; Liu, Y.; Ruoff, R.S.; Lei, W. Functionalized boron nitride membranes with ultrafast solvent transport performance for molecular separation. *Nat. Commun.* **2018**, *9*, 1902. [CrossRef]
56. Kojima, A.; Teshima, K.; Shirai, Y.; Miyasaka, T. Organometal Halide Perovskites as Visible-Light Sensitizers for Photovoltaic Cells. *J. Am. Chem. Soc.* **2009**, *31*, 6050–6051. [CrossRef]
57. Wu, M.; Zhang, Q.; Fang, Y.; Deng, C.; Zhou, F.; Zhang, Y.; Wang, X.; Tang, Y.; Wang, Y. Polylysine-modified MXene nanosheets with highly loaded glucose oxidase as cascade nanoreactor for glucose decomposition and electrochemical sensing. *J. Colloid Interface Sci.* **2021**, *586*, 20–29. [CrossRef]
58. Koyappayil, A.; Chavan, S.G.; Mohammadniaei, M.; Go, A.; Hwang, S.Y.; Lee, M.-H. β-Hydroxybutyrate dehydrogenase decorated MXene nanosheets for the amperometric determination of β-hydroxybutyrate. *Microchim. Acta* **2020**, *187*, 277. [CrossRef]
59. Chia, H.L.; Mayorga-Martinez, C.C.; Antonatos, N.; Sofer, Z.; Gonzalez-Julian, J.J.; Webster, R.D.; Pumera, M. MXene Titanium Carbide-based Biosensor: Strong Dependence of Exfoliation Method on Performance. *Anal. Chem.* **2020**, *92*, 2452–2459. [CrossRef] [PubMed]
60. Zhao, F.; Yao, Y.; Jiang, C.; Shao, Y.; Barceló, D.; Ying, Y.; Ping, J. Self-reduction bimetallic nanoparticles on ultrathin MXene nanosheets as functional platform for pesticide sensing. *J. Hazard. Mater.* **2020**, *384*, 121358. [CrossRef]
61. Yu, L.; Bati, A.S.R.; Grace, T.S.L.; Batmunkh, M.; Shapter, J.G. $Ti_3C_2T_x$ (MXene)-Silicon Heterojunction for Efficient Photovoltaic Cells. *Adv. Energy Mater.* **2019**, *9*, 1901063. [CrossRef]
62. Zhang, C.F.J.; Pinilla, S.; McEyoy, N.; Cullen, C.P.; Anasori, B.; Long, E.; Park, S.H.; Seral-Ascaso, A.; Shmeliov, A.; Krishnan, D.; et al. Oxidation Stability of Colloidal Two-Dimensional Titanium Carbides (MXenes). *Chem. Mater.* **2017**, *29*, 4848–4856.
63. Yang, L.; Dall'Agnese, C.; Dall'Agnese, Y.; Chen, G.; Gao, Y.; Sanehira, Y.; Jena, A.K.; Wang, X.-F.; Gogotsi, Y.; Miyasaka, T. Surface-Modified Metallic $Ti_3C_2T_x$ MXene as Electron Transport Layer for Planar Heterojunction Perovskite Solar Cells. *Adv. Funct. Mater.* **2019**, *29*, 1905694. [CrossRef]
64. Srivastava, P.; Mishra, A.; Mizuseki, H.; Lee, K.R.; Singh, A.K. Mechanistic Insight into the Chemical Exfoliation and Functionalization of Ti_3C_2 MXene. *ACS Appl. Mater. Interfaces* **2016**, *8*, 24256–24264. [CrossRef]
65. Khazaei, M.; Mishra, A.; Venkataramanan, N.S.; Singh, A.K.; Yunoki, S. Recent Advances in MXenes: From Fundamentals to Applications. *Curr. Opin. Solid State Mater. Sci.* **2019**, *23*, 164–178. [CrossRef]
66. Xiong, D.; Li, X.; Bai, Z.; Lu, S. Recent Advances in Layered $Ti_3C_2T_x$ MXene for Electrochemical Energy Storage. *Small* **2018**, *14*, 1703419. [CrossRef] [PubMed]
67. Halim, J.; Lukatskaya, M.R.; Cook, K.M.; Lu, J.; Smith, C.R.; Naslund, L.A.; May, S.J.; Hultman, L.; Gogotsi, Y.; Eklund, P.; et al. Transparent Conductive Two-Dimensional Titanium Carbide Epitaxial Thin Films. *Chem. Mater.* **2014**, *26*, 2374–2381. [CrossRef]
68. Ghidiu, M.; Lukatskaya, M.R.; Zhao, M.Q.; Gogotsi, Y.; Barsoum, M.W. Conductive Two-Dimensional Titanium Carbide 'Clay' with High Volumetric Capacitance. *Nature* **2014**, *516*, 78–81. [CrossRef] [PubMed]
69. Lipatov, A.; Alhabeb, M.; Lukatskaya, M.R.; Boson, A.; Gogotsi, Y.; Sinitskii, A. Effect of Synthesis on Quality, Electronic Properties and Environmental Stability of Individual Monolayer Ti_3C_2 MXene Flakes. *Adv. Electron. Mater.* **2016**, *2*, 1600255. [CrossRef]
70. Urbankowski, P.; Anasori, B.; Makaryan, T.; Er, D.; Kota, S.; Walsh, P.L.; Zhao, M.; Shenoy, V.B.; Barsoum, M.W.; Gogotsi, Y. Synthesis of Two-Dimensional Titanium Nitride Ti_4N_3 (MXene). *Nanoscale* **2016**, *8*, 11385–11391. [CrossRef]
71. Mashtalir, O.; Naguib, M.; Mochalin, V.N.; Dall'Agnese, Y.; Heon, M.; Barsoum, M.W.; Gogotsi, Y. Intercalation and Delamination of Layered Carbides and Carbonitrides. *Nat. Commun.* **2013**, *4*, 1716. [CrossRef] [PubMed]
72. Anasori, B.; Lukatskaya, M.R.; Gogotsi, Y. 2D Metal Carbides and Nitrides (MXenes) for Energy Storage. *Nat. Rev. Mater.* **2017**, *2*, 16098. [CrossRef]
73. Maleski, K.; Mochalin, V.N.; Gogotsi, Y. Dispersions of Two-Dimensional Titanium Carbide MXene in Organic Solvents. *Chem. Mater.* **2017**, *29*, 1632–1640. [CrossRef]
74. Mashtalir, O.; Lukatskaya, M.R.; Kolesnikov, A.I.; Raymundo-Pinero, E.; Naguib, M.; Barsoum, M.W.; Gogotsi, Y. The Effect of Hydrazine Intercalation on the Structure and Capacitance of 2D Titanium Carbide (MXene). *Nanoscale* **2016**, *8*, 9128–9133. [CrossRef]
75. Yazdanparast, S.; Soltanmohammad, S.; Fash-White, A.; Tucker, G.J.; Brennecka, G.L. Synthesis and Surface Chemistry of 2D TiVC Solid-Solution MXenes. *ACS Appl. Mater. Interfaces* **2020**, *12*, 20129–20137. [CrossRef] [PubMed]
76. Mondal, K.; Ghosh, P. Exfoliation of Ti2C and Ti3C2 Mxenes from bulk trigonal phases of titanium carbide: A theoretical prediction. *Solid State Commun.* **2019**, *299*, 113657. [CrossRef]
77. Guo, Z.; Gao, L.; Xu, Z.; Teo, S.; Zhang, C.; Kamata, Y.; Hayase, S.; Ma, T. High Electrical Conductivity 2D MXene Serves as Additive of Perovskite for Efficient Solar Cells. *Small* **2018**, *14*, 1802738. [CrossRef]
78. Agresti, A.; Pazniak, A.; Pescetelli, S.; Vito, A.D.; Rossi, D.; Pecchia, A.; Maur, M.A.; Liedl, A.; Larciprete, R.; Kuznetsov, D.; et al. Titanium-carbide MXenes for work function and interface engineering in perovskite solar cells. *Nat. Mater.* **2019**, *18*, 1228–1234. [CrossRef] [PubMed]
79. Cao, J.; Meng, F.; Gao, L.; Yang, S.; Yan, Y.; Wang, N.; Liu, A.; Li, Y.; Ma, T. Alternative electrodes for HTMs and noble-metal free perovskite solar cells: 2D MXenes electrodes. *RSC Adv.* **2019**, *9*, 34152–34157. [CrossRef]

80. Zhang, Z.; Li, Y.; Liang, C.; Yu, G.; Zhao, J.; Luo, S.; Huang, Y.; Su, C.; Xing, G. In Situ Growth of $MAPbBr_3$ Nanocrystals on Few-Layer MXene Nanosheets with Efficient Energy Transfer. *Small* **2020**, *16*, 1905896. [CrossRef]
81. Chen, X.; Xu, W.; Ding, N.; Ji, Y.; Pan, G.; Zhu, J.; Zhou, D.; Wu, Y.; Chen, C.; Song, H. Dual Interfacial Modification Engineering with 2D MXene Quantum Dots and Copper Sulphide Nanocrystals Enabled High-Performance Perovskite Solar Cells. *Adv. Funct. Mater.* **2020**, *30*, 2003295. [CrossRef]
82. Yang, L.; Dall'Agnese, Y.; Hantanasirisakul, K.; Shuck, C.E.; Maleski, K.; Alhabeb, M.; Chen, G.; Gao, Y.; Sanehira, Y.; Jena, A.K.; et al. SnO_2-Ti_3C_2 MXene electron transport layers for perovskite solar cells. *J. Mater. Chem. A* **2019**, *7*, 5635–5642. [CrossRef]
83. Huang, L.; Zhou, X.; Xue, R.; Xu, P.; Wang, S.; Xu, C.; Zeng, W.; Xiong, Y.; Sang, H.; Liang, D. Low-Temperature Growing Anatase TiO_2/SnO_2 Multi-dimensional Heterojunctions at MXene Conductive Network for High-Efficient Perovskite Solar Cells. *Nano-Micro Lett.* **2020**, *12*, 44. [CrossRef] [PubMed]
84. Wang, Y.; Xiang, P.; Ren, A.; Lai, H.; Zhang, Z.; Xuan, Z.; Wan, Z.; Zhang, J.; Hao, X.; Wu, L.; et al. MXene-Modulated Electrode/SnO_2 Interface Boosting Charge Transport in Perovskite Solar Cells. *ACS Appl. Mater. Interfaces* **2020**, *12*, 53973–53983. [CrossRef] [PubMed]
85. Yang, L.; Kan, D.; Dall'Agnese, C.; Dall'Agnese, Y.; Wang, B.; Jena, A.K.; Wei, Y.; Chen, G.; Wang, X.-F.; Gogotsi, Y.; et al. Performance improvement of MXene-based perovskite solar cells upon property transition from metallic to semiconductive by oxidation of $Ti_3C_2T_x$ in air. *J. Mater. Chem. A* **2021**, *9*, 5016–5025. [CrossRef]
86. Jin, X.; Yang, L.; Wang, X.F. Efficient Two-Dimensional Perovskite Solar Cells Realized by Incorporation of $Ti_3C_2T_x$ MXene as Nano-Dopants. *Nano-Micro Lett.* **2021**, *13*, 68. [CrossRef] [PubMed]
87. Ge, J.; Li, W.; He, X.; Chen, H.; Fang, W.; Du, X.; Li, Y.; Zhao, L. Charge behavior modulation by titanium-carbide quantum dots and nanosheets for efficient perovskite solar cells. *Mater. Today Energ.* **2020**, *18*, 100562. [CrossRef]
88. Saranin, D.; Pescetelli, S.; Pazniak, A.; Rossi, D.; Liedl, A.; Yakusheva, A.; Luchnikov, L.; Podgorny, D.; Gostischev, P.; Didenko, S.; et al. Transition metal carbides (MXenes) for efficient NiO-based inverted perovskite solar cells. *Nano Energy* **2021**, *82*, 105771. [CrossRef]
89. Zhao, Y.; Zhang, X.; Han, X.; Hou, C.; Wang, H.; Qi, J.; Li, Y.; Zhang, Q. Tuning the reactivity of PbI_2 film via monolayer $Ti_3C_2T_x$ MXene for two-step-processed $CH_3NH_3PbI_3$ solar cells. *Chem. Eng. J.* **2021**, *417*, 127912. [CrossRef]
90. Yang, Y.; Lu, H.; Feng, S.; Yang, L.; Dong, H.; Wang, J.; Tian, C.; Li, L.; Lu, H.; Jeong, J.; et al. Modulation of perovskite crystallization processes towards highly efficient and stable perovskite solar cells with MXene quantum dot-modified SnO_2. *Energy Environ. Sci.* **2021**, *14*, 3447–3454. [CrossRef]
91. Li, Z.; Wang, P.; Ma, C.; Igbari, F.; Kang, Y.; Wang, K.-L.; Song, W.; Dong, C.; Li, Y.; Yao, J.; et al. Single-Layered MXene Nanosheets Doping TiO_2 for Efficient and Stable Double Perovskite Solar Cells. *J. Am. Chem. Soc.* **2021**, *143*, 2593–2600. [CrossRef]
92. Chen, T.; Tong, G.; Xu, E.; Li, H.; Li, P.; Zhu, Z.; Tang, J.; Qi, Y.; Jiang, Y. Accelerating hole extraction by inserting 2D Ti_3C_2-MXene interlayer to all inorganic perovskite solar cells with long-term stability. *J. Mater. Chem. A* **2019**, *7*, 20597–20603. [CrossRef]
93. Mi, L.; Zhang, Y.; Chen, T.; Xu, E.; Jiang, Y. Carbon electrode engineering for high efficiency all-inorganic perovskite solar cells. *RSC Adv.* **2020**, *10*, 12298–12303. [CrossRef] [PubMed]
94. Zhang, Y.-Z.; Wang, Y.; Jiang, Q.; El-Demellawi, J.K.; Kim, H.; Alshareef, H.N. MXene Printing and Patterned Coating for Device Applications. *Adv. Mater.* **2020**, *32*, 1908486. [CrossRef]
95. Mathew, M.; Radhakrishnan, S.; Vaidyanathan, A.; Chakraborty, B.; Rout, C.S. Flexible and wearable electrochemical biosensors based on two-dimensional materials: Recent developments. *Anal. Bioanal. Chem.* **2021**, *413*, 727–762. [CrossRef]
96. Huang, W.; Hu, L.; Tang, Y.; Xie, Z.; Zhang, H. Recent Advances in Functional 2D MXene-Based Nanostructures for Next-Generation Devices. *Adv. Funct. Mater.* **2020**, *30*, 2005223. [CrossRef]
97. Fang, D.; Zhao, D.; Zhang, S.; Huang, Y.; Dai, H.; Lin, Y. Black phosphorus quantum dots functionalized MXenes as the enhanced dual-mode probe for exosomes sensing. *Sens. Actuators B Chem.* **2020**, *305*, 127544. [CrossRef]
98. Feng, A.; Yu, Y.; Wang, Y.; Jiang, F.; Yu, Y.; Mi, L.; Song, L. Two-dimensional MXene Ti_3C_2 produced by exfoliation of Ti_3AlC_2, Mater. *Design* **2017**, *114*, 161–166.
99. Wang, F.; Yang, C.; Duan, C.; Xiao, D.; Tang, Y.; Zhu, J. An Organ-Like Titanium Carbide Material (MXene) with Multilayer Structure Encapsulating Hemoglobin for a Mediator-Free Biosensor. *J. Electrochem. Soc.* **2015**, *162*, B16–B21. [CrossRef]
100. Zhou, L.Y.; Zhang, X.; Ma, L.; Gao, J.; Jiang, Y.J. Acetylcholinesterase/chitosan-transition metal carbides nanocomposites-based biosensor for the organophosphate pesticides detection. *Biochem. Eng. J.* **2017**, *128*, 243–249. [CrossRef]
101. Wu, L.X.; Lu, X.; Dhanjai, X.B.; Wu, Z.S.; Dong, Y.F.; Wang, X.H.; Zheng, S.H.; Chen, J.P. 2D transition metal carbide MXene as a robust biosensing platform for enzyme immobilization and ultrasensitive detection of phenol. *Biosens. Bioelectron.* **2018**, *107*, 69–75. [CrossRef] [PubMed]
102. Wang, F.; Yang, C.; Duan, M.; Tang, Y.; Zhu, J. TiO_2 nanoparticle modified organ-like Ti_3C_2 MXene nanocomposite encapsulating hemoglobin for a mediator-free biosensor with excellent performances. *Biosens. Bioelectron.* **2015**, *74*, 1022–1028. [CrossRef] [PubMed]
103. Rakhi, R.B.; Nayak, P.; Xia, C.; Alshareef, H.N. Novel amperometric glucose biosensor based on MXene nanocomposite. *Sci. Rep.* **2016**, *6*, 36422. [CrossRef] [PubMed]
104. Jiang, Y.J.; Zhang, X.N.; Pei, L.J.; Yue, S.; Ma, L.; Zhou, L.Y.; Huang, Z.H.; He, Y.; Gao, J. Silver nanoparticles modified two-dimensional transition metal carbides as nanocarriers to fabricate acetycholinesterase-based electrochemical biosensor. *Chem. Eng. J.* **2018**, *339*, 547–556. [CrossRef]

105. Song, D.D.; Jiang, X.Y.; Li, Y.S.; Lu, X.; Luan, S.R.; Wang, Y.Z.; Li, Y.; Gao, F.M. Metal−organic frameworks-derived MnO_2/Mn_3O_4 microcuboids with hierarchically ordered nanosheets and Ti_3C_2 MXene/Au NPs composites for electrochemical pesticide detection. *J. Hazard. Mater.* **2019**, *373*, 367–376. [CrossRef] [PubMed]
106. Wang, G.X.; Sun, J.F.; Yao, Y.; An, X.S.; Zhang, H.; Chu, G.L.; Jiang, S.; Guo, Y.M.; Sun, X.; Liu, Y. Detection of Inosine Monophosphate (IMP) in Meat Using Double-Enzyme Sensor. *Food Anal. Meth.* **2020**, *13*, 420–432. [CrossRef]
107. Zheng, J.; Diao, J.; Jin, Y.; Ding, A.; Wang, B.; Wu, L.; Weng, B.; Chen, J. An Inkjet Printed Ti_3C_2-GO Electrode for the Electrochemical Sensing of Hydrogen Peroxide. *J. Electrochem. Soc.* **2018**, *165*, B227–B231. [CrossRef]
108. Neampet, S.; Ruecha, N.; Qin, J.; Wonsawat, W.; Chailapakul, O.; Rodthongkum, N. A nanocomposite prepared from platinum particles, polyaniline and a Ti_3C_2 MXene for amperometric sensing of hydrogen peroxide and lactate. *Microchim. Acta* **2019**, *186*, 752. [CrossRef]
109. Rasheed, P.A.; Pandey, R.P.; Rasool, K.; Mahmoud, K.A. Ultra-sensitive electrocatalytic detection of bromate in drinking water based on Nafion/$Ti_3C_2T_x$ (MXene) modified glassy carbon electrode. *Sens. Actuators B Chem.* **2018**, *265*, 652–659. [CrossRef]
110. Wu, D.H.; Wu, M.Y.; Yang, J.H.; Zhang, H.W.; Xie, K.F.; Lin, C.T.; Yu, A.M.; Yu, J.H.; Fu, L. Delaminated $Ti_3C_2T_x$ (MXene) for electrochemical carbendazim sensing. *Mater. Lett.* **2019**, *236*, 412–415. [CrossRef]
111. Shahzad, F.; Iqbal, A.; Zaidi, S.A.; Hwang, S.W.; Koo, C.M. Nafion-stabilized two-dimensional transition metal carbide ($Ti_3C_2T_x$ MXene) as a high-performance electrochemical sensor for neurotransmitter. *J. Ind. Eng. Chem.* **2019**, *79*, 338–344. [CrossRef]
112. Pham, T.S.H.; Fu, L.; Mahon, P.; Lai, G.; Yu, A. Fabrication of β-Cyclodextrin-Functionalized Reduced Graphene Oxide and Its Application for Electrocatalytic Detection of Carbendazim. *Electrocatalysis* **2016**, *7*, 411–419. [CrossRef]
113. Shankar, S.S.; Shereema, R.M.; Rakhi, R.B. Electrochemical Determination of Adrenaline Using MXene/Graphite Composite Paste Electrodes. *ACS Appl. Mater. Interfaces* **2018**, *10*, 43343–43351. [CrossRef]
114. Zhang, Y.; Jiang, X.T.; Zhang, J.J.; Zhang, H.; Li, Y.C. Simultaneous voltammetric determination of acetaminophen and isoniazid using MXene modified screen-printed electrode. *Biosens. Bioelectron.* **2019**, *130*, 315–321. [CrossRef] [PubMed]
115. Ramachandran, R.; Zhao, C.; Rajkumar, M.; Rajavel, K.; Zhu, P.; Xuan, W.; Xu, Z.-X.; Wang, F. Porous nickel oxide microsphere and $Ti_3C_2T_x$ hybrid derived from metal-organic framework for battery-type supercapacitor electrode and non-enzymatic H_2O_2 sensor. *Electrochim. Acta* **2019**, *322*, 134771. [CrossRef]
116. Li, M.; Fang, L.; Zhou, H.; Wu, F.; Lu, Y.; Luo, H.; Zhang, Y.; Hu, B. Three-dimensional porous MXene/NiCo-LDH composite for high performance non-enzymatic glucose sensor. *Appl. Surf. Sci.* **2019**, *495*, 143554. [CrossRef]
117. Zou, H.Y.; Zhang, F.F.; Wang, H.Y.; Xia, J.F.; Gao, L.N.; Wang, Z.H. Au nanoparticles supported on functionalized two-dimensional titanium carbide for the sensitive detection of nitrite. *New J. Chem.* **2019**, *43*, 2464–2470. [CrossRef]
118. Rasheed, P.A.; Pandey, R.P.; Jabbar, K.A.; Ponraj, J.; Mahmoud, K.A. Sensitive electrochemical detection of l-cysteine based on a highly stable Pd@$Ti_3C_2T_x$ (MXene) nanocomposite modified glassy carbon electrode. *Anal. Methods* **2019**, *11*, 3851–3856. [CrossRef]
119. Zheng, J.; Wang, B.; Jin, Y.; Weng, B.; Chen, J. Nanostructured MXene-based biomimetic enzymes for amperometric detection of superoxide anions from HepG2 cells. *Microchim. Acta* **2019**, *186*, 95. [CrossRef]
120. Huang, R.; Chen, S.; Yu, J.; Jiang, X. Self-assembled $T_{i3}C_2$/MWCNTs nanocomposites modified glassy carbon electrode for electrochemical simultaneous detection of hydroquinone and catechol. *Ecotoxicol. Environ. Saf.* **2019**, *184*, 109619. [CrossRef]
121. Zhang, R.Y.; Liu, J.; Li, Y.C. MXene with Great Adsorption Ability toward Organic Dye: An Excellent Material for Constructing a Ratiometric Electrochemical Sensing Platform. *ACS Sens.* **2019**, *4*, 2058–2064. [CrossRef]
122. Tu, X.; Gao, F.; Ma, X.; Zou, J.; Yu, Y.; Li, M.; Qu, F.; Huang, X.; Lu, L. Mxene/carbon nanohorn/β-cyclodextrin-Metal-organic frameworks as high-performance electrochemical sensing platform for sensitive detection of carbendazim pesticide. *J. Hazard. Mater.* **2020**, *396*, 122776. [CrossRef]
123. Huang, R.; Liao, D.; Chen, S.; Yu, J.; Jiang, X. A strategy for effective electrochemical detection of hydroquinone and catechol: Decoration of alkalization-intercalated Ti_3C_2 with MOF-derived N-doped porous carbon. *Sens. Actuators B Chem.* **2020**, *320*, 128386. [CrossRef]
124. Ma, X.; Tu, X.; Gao, F.; Xie, Y.; Huang, X.; Fernandez, C.; Qu, F.; Liu, G.; Lu, L.; Yu, Y. Hierarchical porous MXene/amino carbon nanotubes-based molecular imprinting sensor for highly sensitive and selective sensing of fisetin. *Sens. Actuators B Chem.* **2020**, *309*, 127815. [CrossRef]
125. Dang, Y.; Guan, X.; Zhou, Y.; Hao, C.; Zhang, Y.; Chen, S.; Ma, Y.; Bai, Y.; Gong, Y.; Gao, Y. Biocompatible PB/Ti_3C_2 hybrid nanocomposites for the non-enzymatic electrochemical detection of H_2O_2 released from living cells. *Sens. Actuators B Chem.* **2020**, *319*, 128259. [CrossRef]
126. Kokulnathan, T.; Kumar, E.A.; Wang, T.-J. Design and In Situ Synthesis of Titanium Carbide/Boron Nitride Nanocomposite: Investigation of Electrocatalytic Activity for the Sulfadiazine Sensor. *ACS Sustain. Chem. Eng.* **2020**, *8*, 12471–12481. [CrossRef]
127. Kalambate, P.K.; Dhanjai; Sinha, A.; Li, Y.; Shen, Y.; Huang, Y. An electrochemical sensor for ifosfamide, acetaminophen, domperidone, and sumatriptan based on self-assembled MXene/MWCNT/chitosan nanocomposite thin film. *Microchim. Acta* **2020**, *187*, 402. [CrossRef] [PubMed]
128. Elumalai, S.; Mani, V.; Jeromiyas, N.; Ponnusamy, V.K.; Yoshimura, M. A composite film prepared from titanium carbide $Ti_3C_2T_x$ (MXene) and gold nanoparticles for voltammetric determination of uric acid and folic acid. *Microchim. Acta* **2019**, *187*, 33. [CrossRef]

129. Wang, X.; Li, M.; Yang, S.; Shan, J. A novel electrochemical sensor based on TiO_2–$Ti_3C_2T_x$/CTAB/chitosan composite for the detection of nitrite. *Electrochim. Acta* **2020**, *359*, 136938. [CrossRef]
130. He, Y.; Ma, L.; Zhou, L.; Liu, G.; Jiang, Y.; Gao, J. Preparation and Application of Bismuth/MXene Nano-Composite as Electrochemical Sensor for Heavy Metal Ions Detection. *Nanomaterials* **2020**, *10*, 866. [CrossRef]
131. Yao, Y.Q.; Han, X.H.; Yang, X.H.; Zhao, J.; Chai, C.P. Detection of Hydrazine at MXene/ZIF-8 Nanocomposite Modified Electrode. *Chin. J. Chem.* **2021**, *39*, 330–336. [CrossRef]